Extracting the thermal SZ signal from heterogeneous millimetre data sets

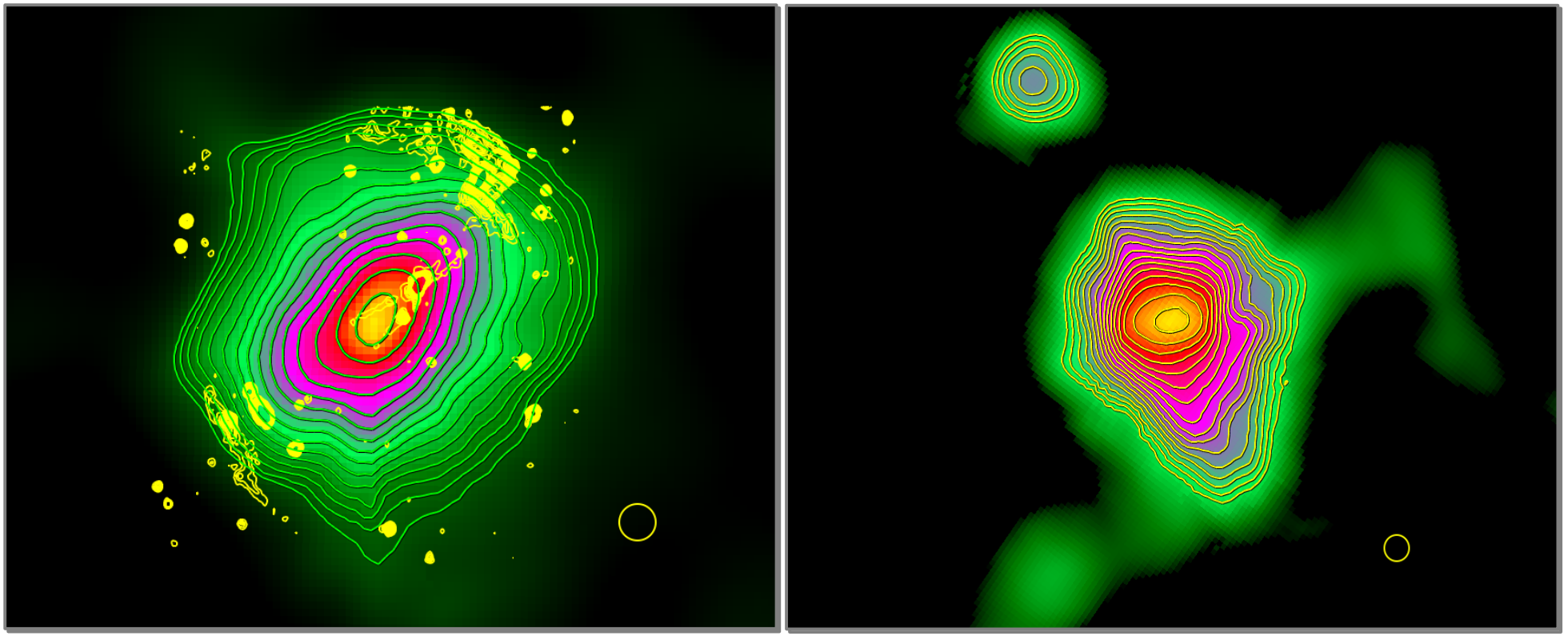

Extracting the thermal SZ signal from heterogeneous millimetre data sets

In col. with: A.S. Baldi, A. Kozmanyan, P. Mazzotta

- Pressure profiles of *Planck* detected clusters;
  - Profile shape and evolution with redshift;
  - Determination of cosmic distances from joined X-ray+SZ studies;
- Cluster maps and substructure detections
- Toward all sky maps of the tSZ background and distant cluster detections

Extended component separation

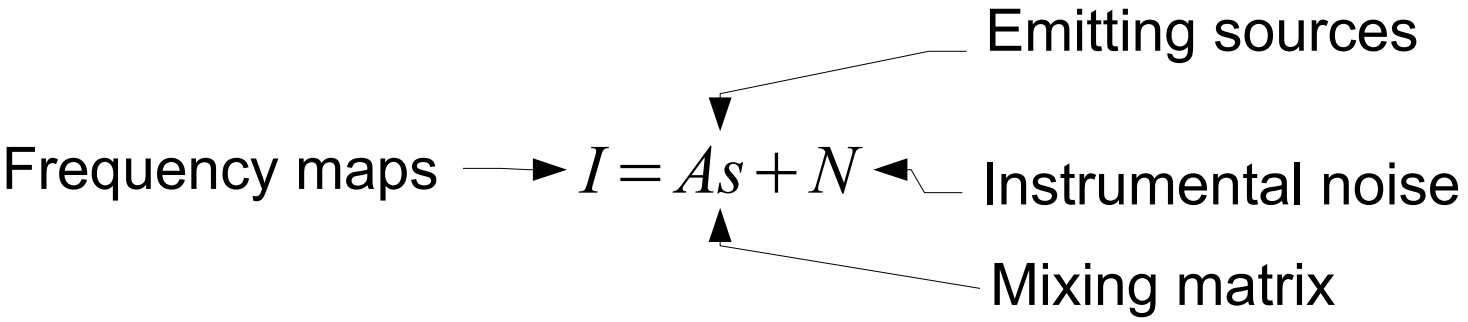

- Best Linear Unbiased Estimates (ILC and derivates) of S;
  - *rely on gaussianity of the foreground fluctuations;*
- Parametric template fitting;
  - *Interesting results for individual localized foregrounds but mapping issues:*
    - *Khatri & Gaspari, 16: Compton y power spectrum in Coma;*
    - *BICEP2+Planck col.: thermal dust polarisation compromises B-mode detections);*
- BSS under sparsity constraint;
  - *Interesting results for CMB mapping but Noise and instrumental nuisance modelling issues:*
    - *Bobin et al, 16 (CMB map closest to 217 GHz map than using ILC based algorithms)*

Pressure profiles of Planck detected clusters

$$I = As + N$$

$$I = A\,\alpha\,\phi + N$$

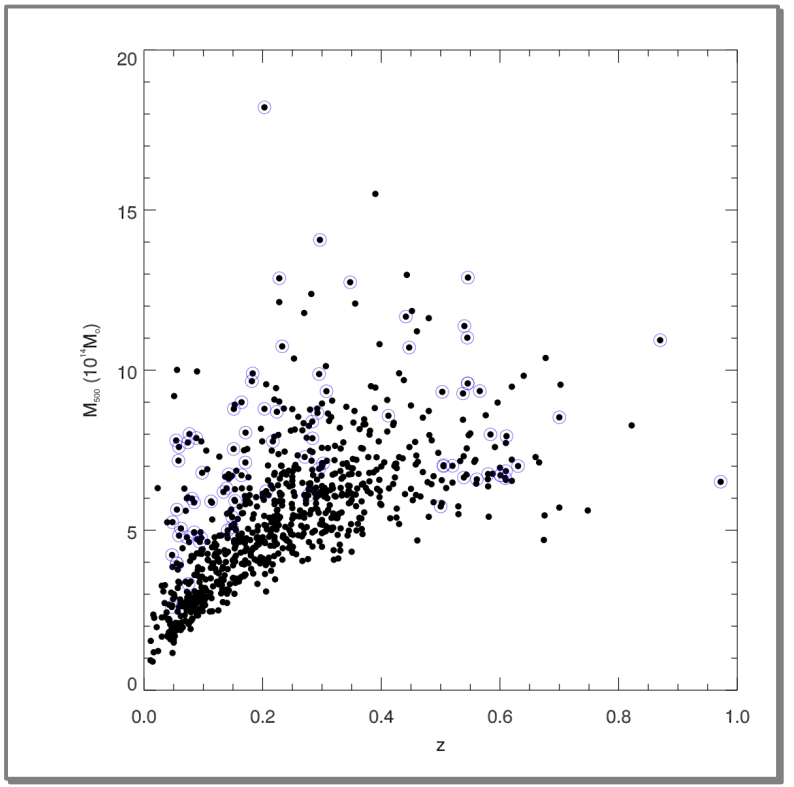

Soft thresholding in a *redundant* wavelet basis:

$$L_1(T, I, \alpha) = \| I - \sum_{s,p \in \Gamma} A_s^p \alpha[p] \phi_p \|_2^2 + T \|\alpha\|_1^1$$

High Frequency Instrument images of Abell 2163 (High-pass filtering)

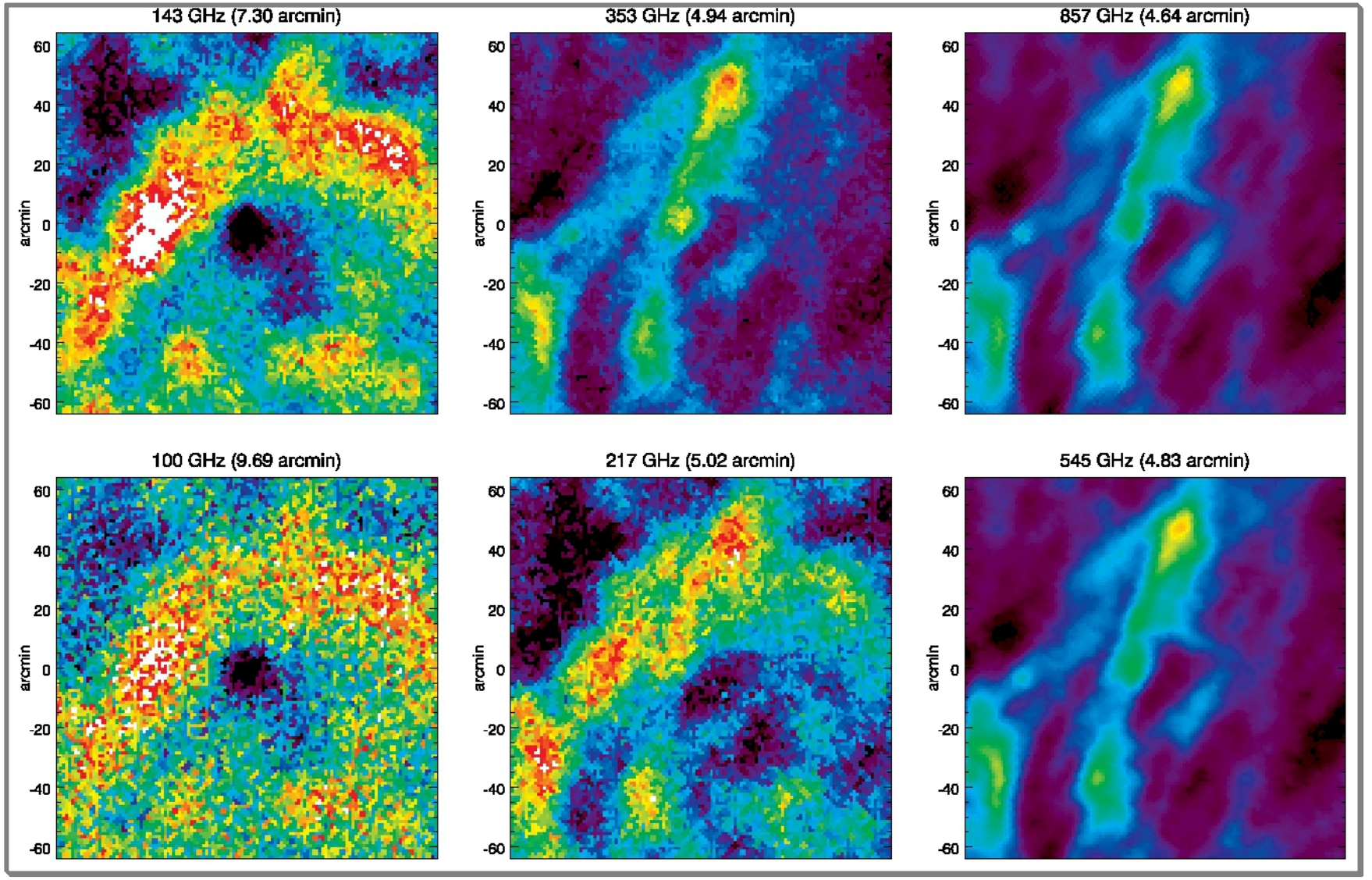

Two components Galactic thermal dust

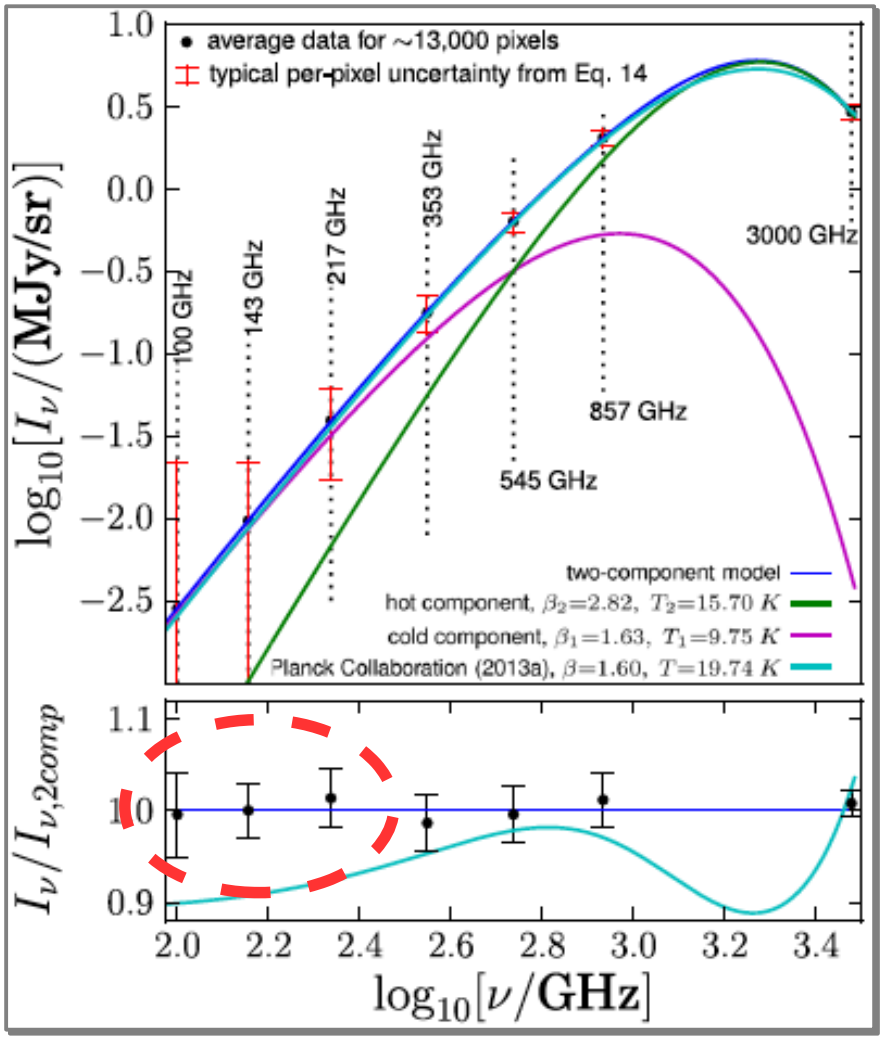

Meisner et Finkbeiner, 15

$$f_{dust} \propto \left[f_1 q_1 \left(\frac{\nu}{\nu_o}\right)^{\beta_1} B_\nu(T_1) + f_2 q_2 \left(\frac{\nu}{\nu_o}\right)^{\beta_2} B_\nu(T_2) \right]$$

- *β_2 assumed constant across the sky;*
- *T2 mapped from HFI + IRAS (100 μm);*
- *T1 = f(T2, β_1,β_2,q_1/q_2);*
- *q_1/q_2 and β_1 left free around each cluster..*

1/3) Thermal dust modelling / subtraction

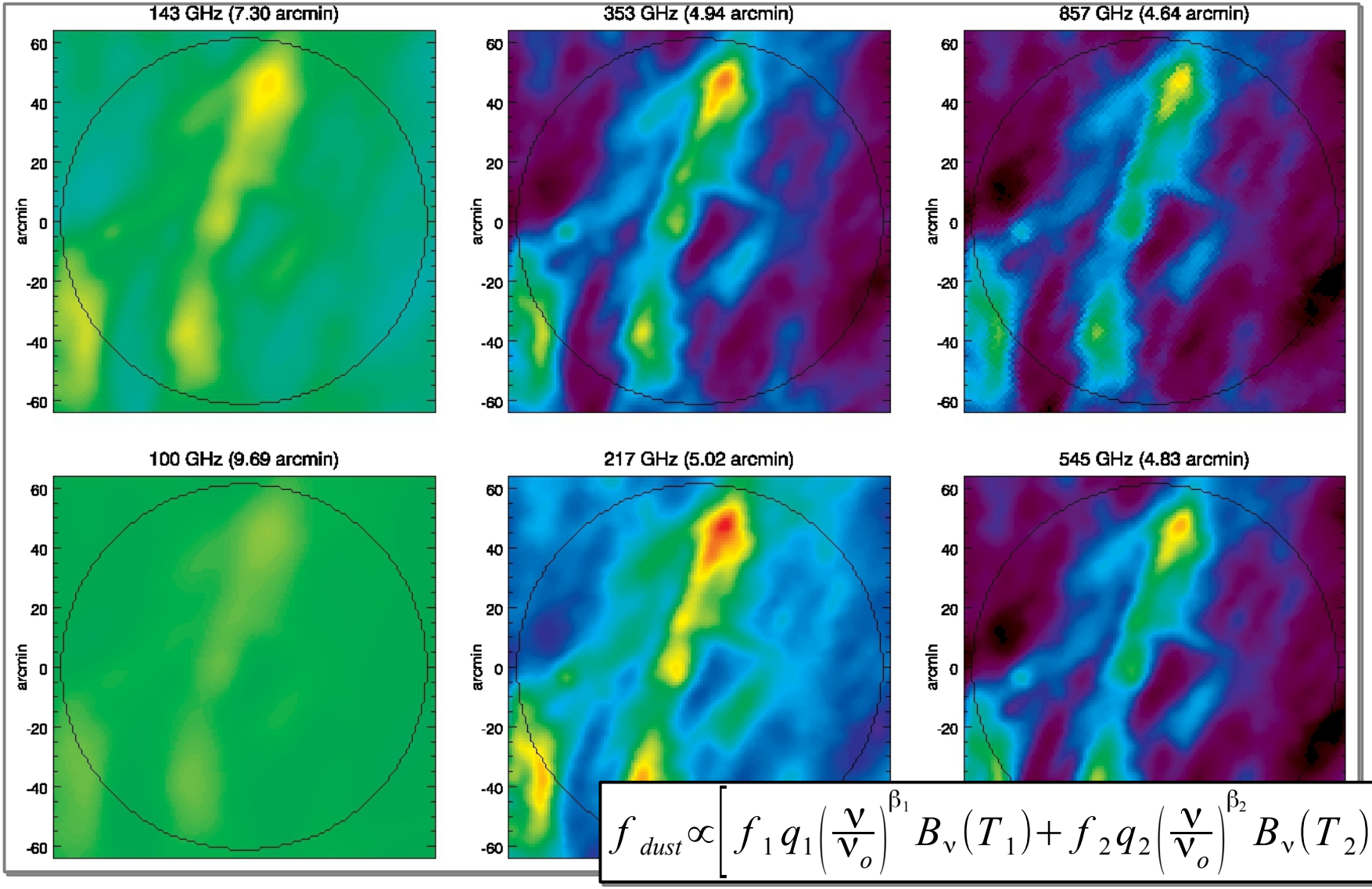

$$f_{dust} \propto \left[f_1 q_1 \left(\frac{\nu}{\nu_o} \right)^{\beta_1} B_\nu(T_1) + f_2 q_2 \left(\frac{\nu}{\nu_o} \right)^{\beta_2} B_\nu(T_2) \right]$$

2/3) CMB modelling / subtraction

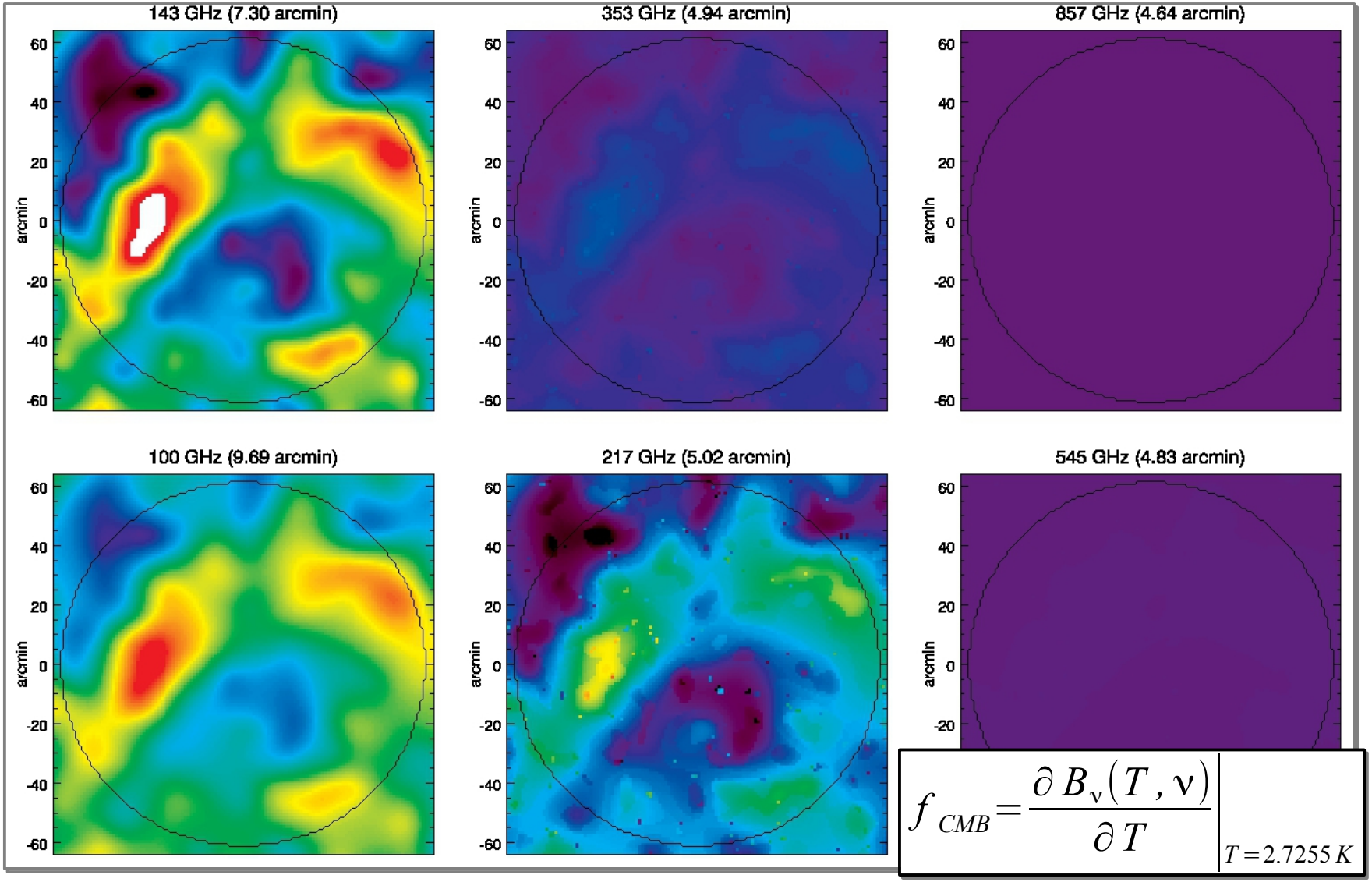

$$f_{CMB} = \frac{\partial B_\nu(T,\nu)}{\partial T}\bigg|_{T=2.7255\,K}$$

3/3) High (spatial) frequencies residua

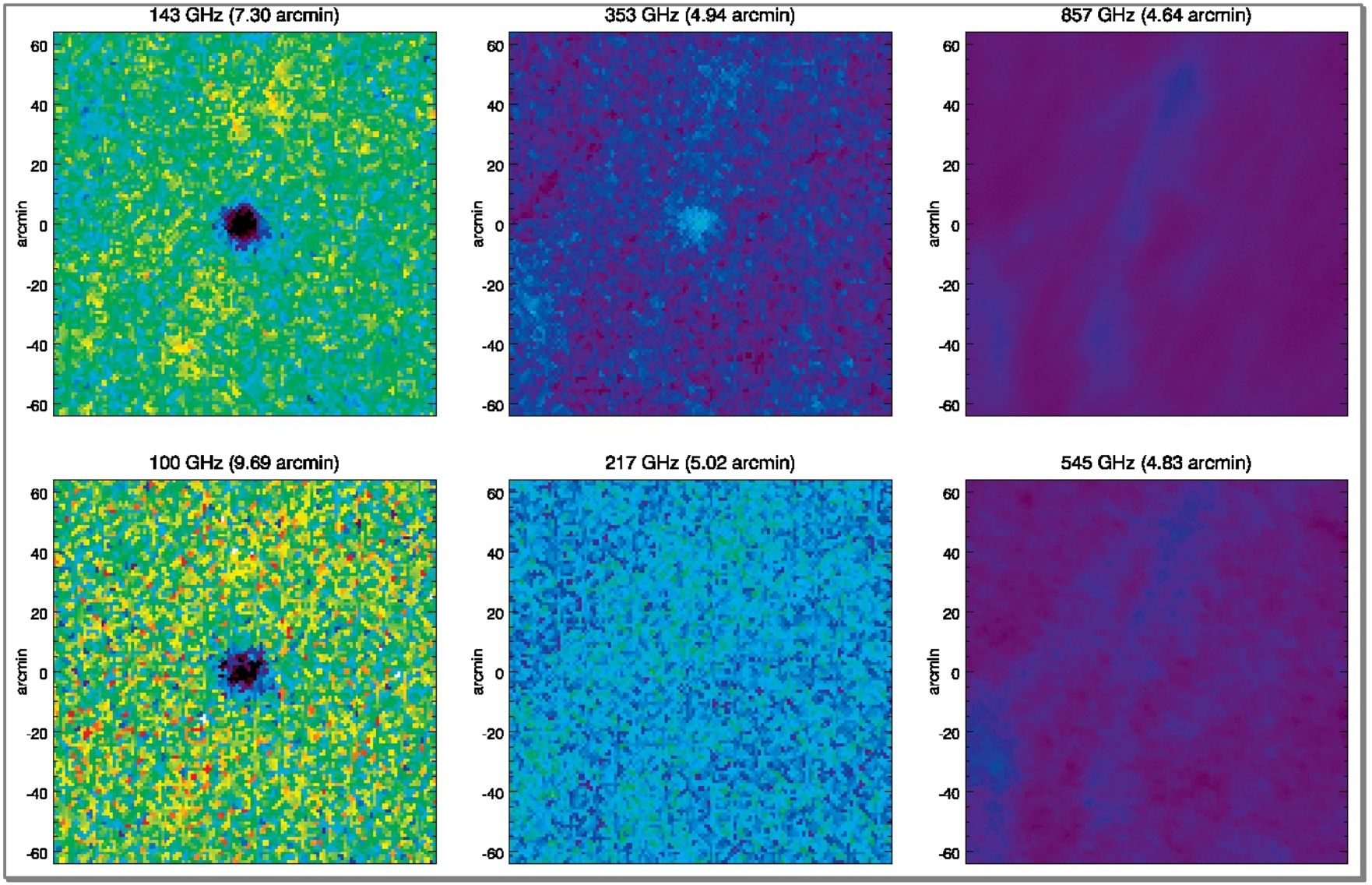

Stacked SZ + CMB + thermal dust signals

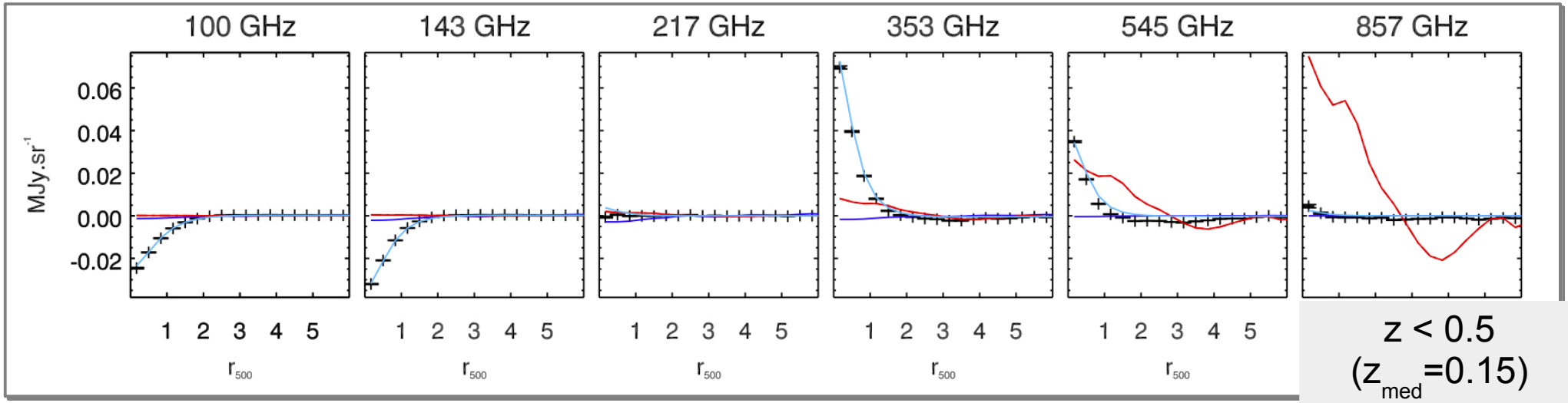

$z < 0.5$
(z_{med}=0.15)

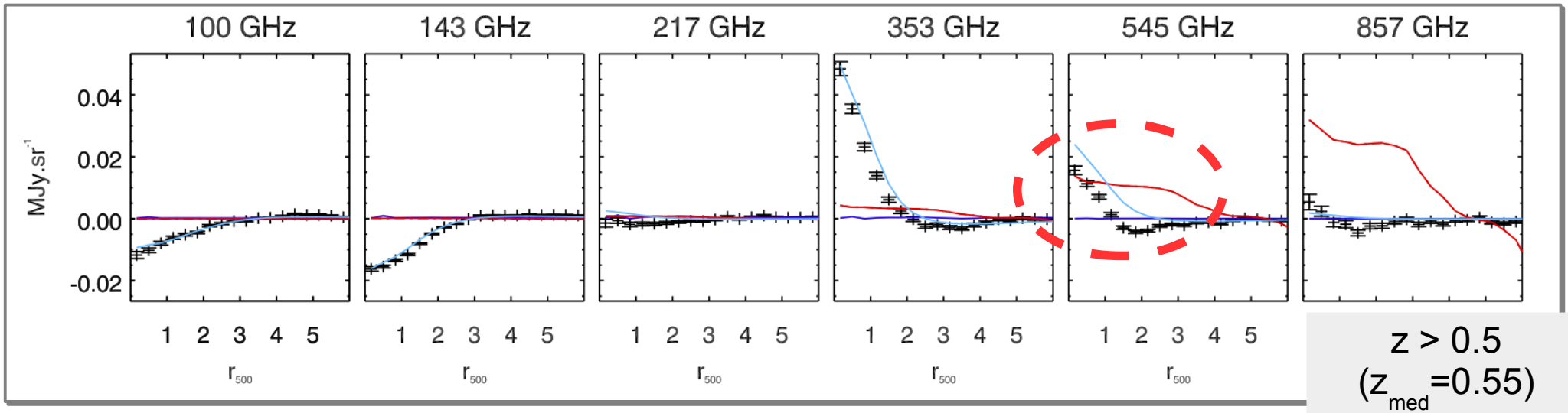

$z > 0.5$
(z_{med}=0.55)

Stacked SZ + CMB + thermal dust signals

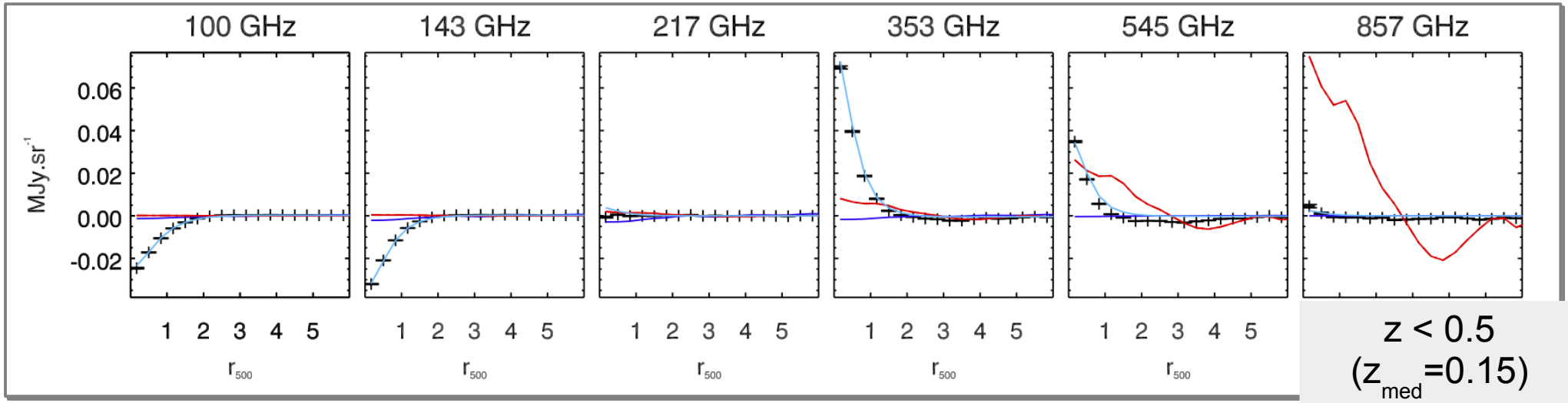

$z < 0.5$
(z_{med}=0.15)

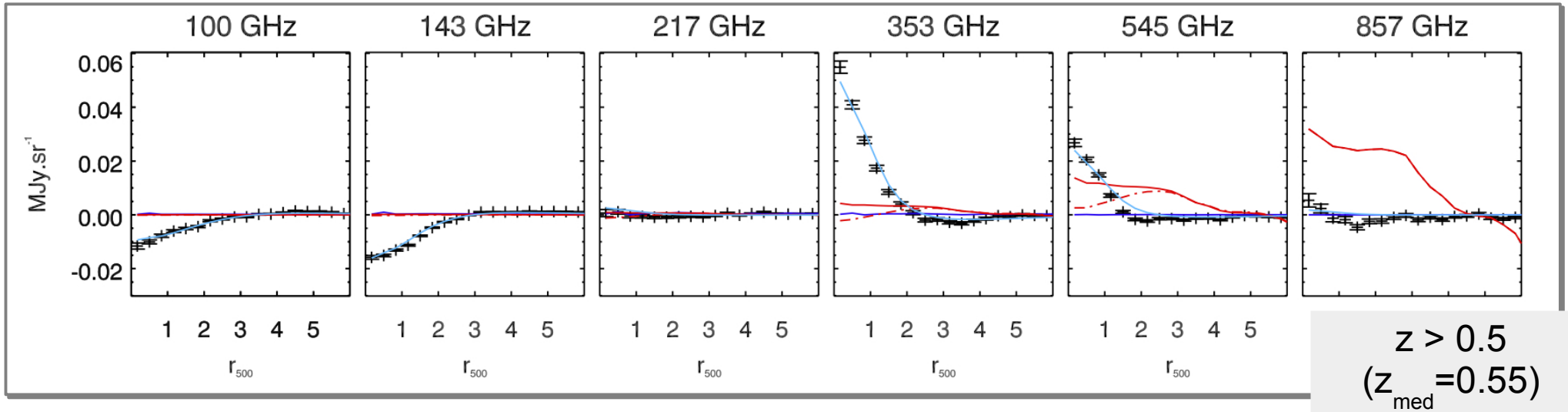

$z > 0.5$
(z_{med}=0.55)

Joined X-ray+SZ estimate of gas pressure profiles

- *Planck Compton parameter*
  --> Gas pressure (Nagai, Kravtsov & Vikhlinin, 07):

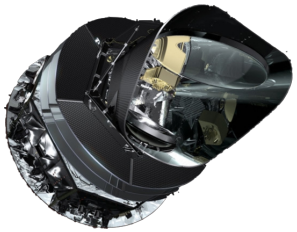

$$P_{500} = 1.45 \times 10^{-12}\, J.m^{-3} \left(\frac{M_{500}}{10^{15} h^{-1} M_{\odot}^{2/3}} \right) E(z)^{8/3}$$

$$\frac{P(r)}{P_{500}} = \frac{P_0}{x^{\gamma}\left(1 + x^{\alpha}\right)^{(\beta-\alpha)/\alpha}}$$

- *X-ray surface brightness ($r<r_{x,max}$)*
  --> Gas density (Vikhlinin et al., 06):

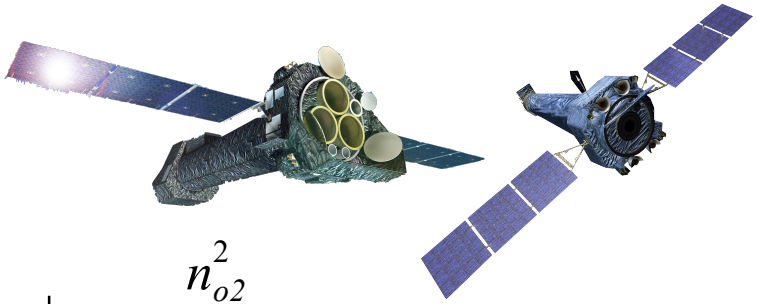

$$n_p n_e = n_o^2 \frac{\left(r/r_c\right)^{-\alpha_1}}{\left(1 + r^2/r_c^2\right)^{(3\beta_1 - \alpha_1/2)}} \frac{1}{\left(1 + r^{\gamma}/r_s^{\gamma}\right)^{\epsilon/\gamma}} + \frac{n_{o2}^2}{\left(1 + r^2/r_{c2}^2\right)^{3\beta_2}}$$

- *Planck Compton parameter + X-ray spectroscopic temperature ($r<r_{x,max}$)*
  --> Ideal gas temperature

$$k\,T(r) = \eta_T \frac{P(r)}{n_e(r)}$$

Mass scaled pressure profiles

$z < 0.5$
(z_{med}=0.15)

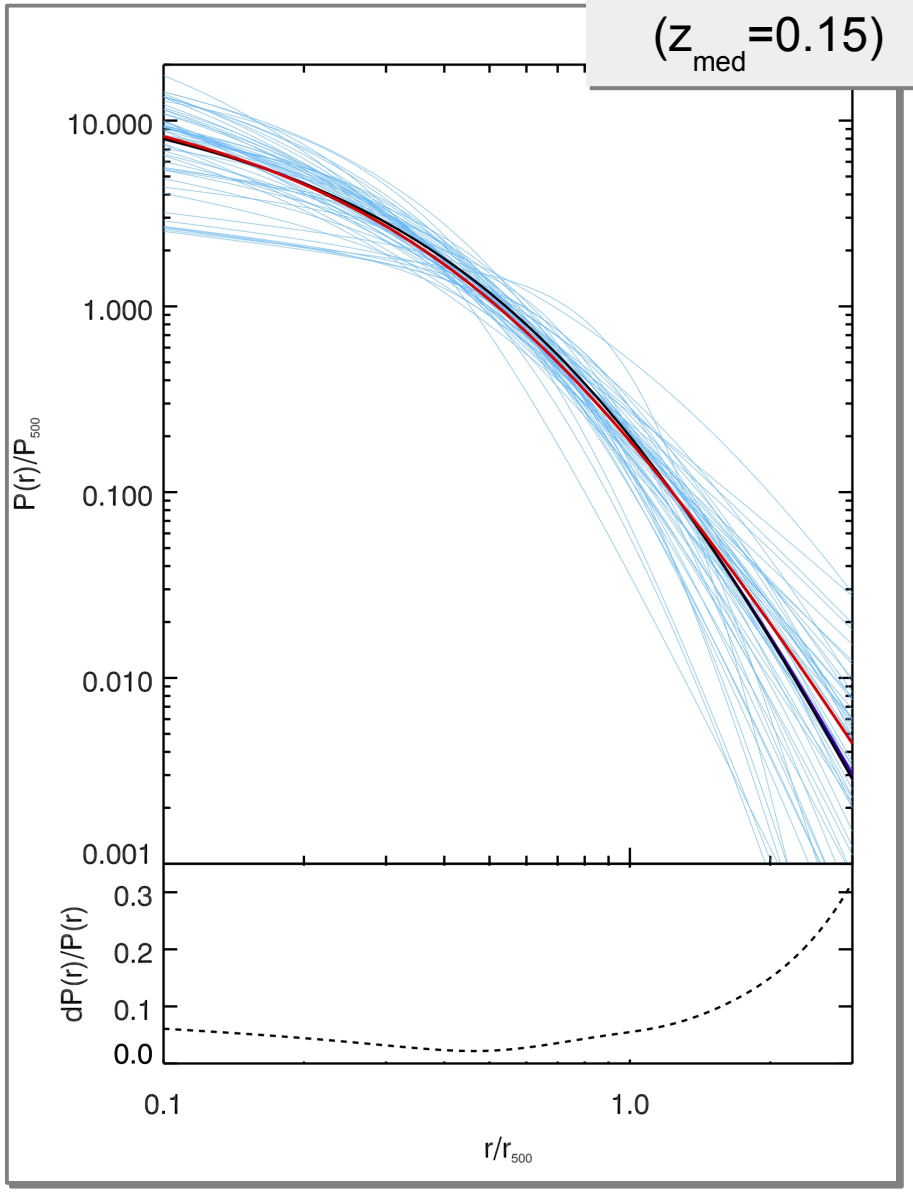

$z > 0.5$
(z_{med}=0.55)

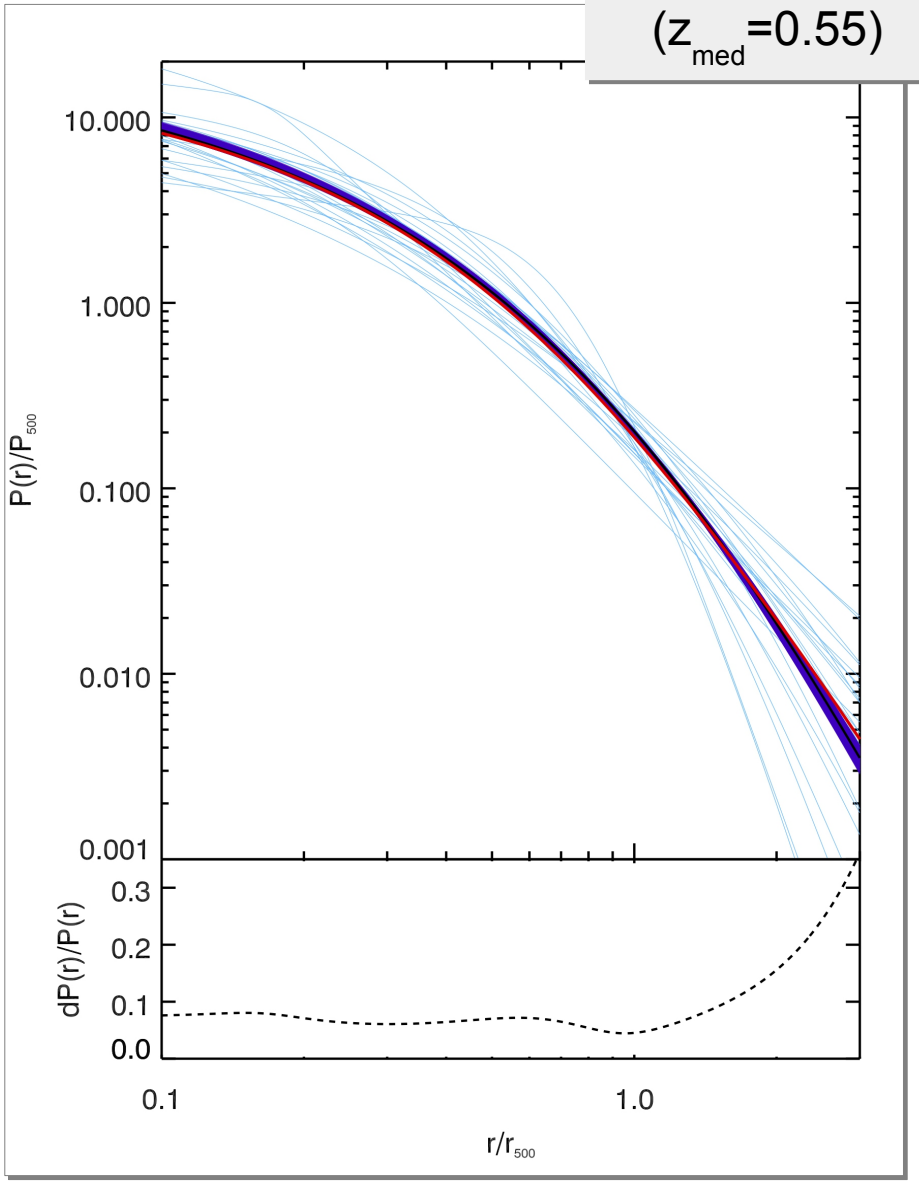

Stacked (mass scaled) pressure profiles

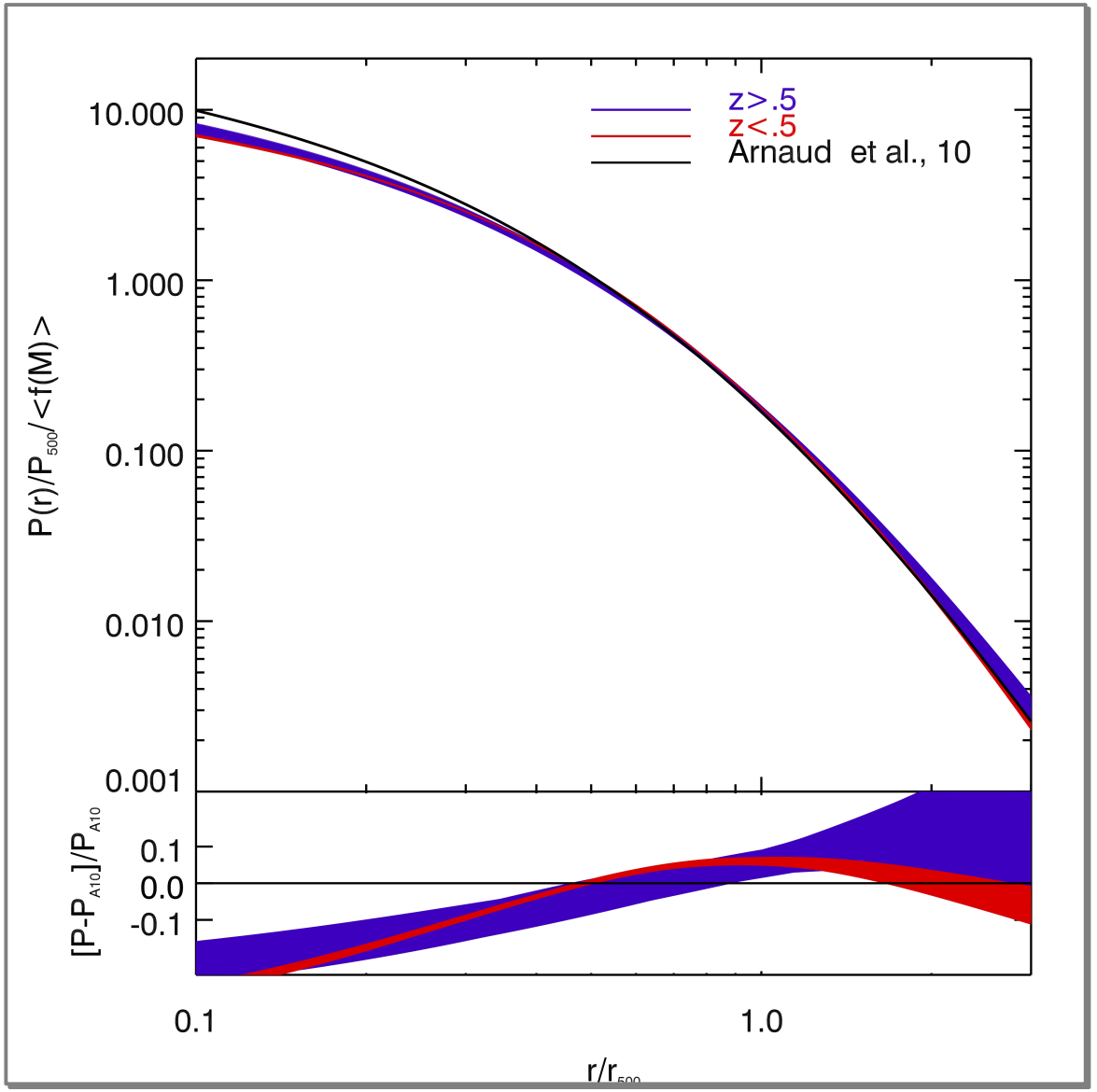

- *High and low redshift subsamples:*
  - *z<0.5;* $\tilde{M} = 7.2\,10^{14}\,M_o$

    z>0.5; $\tilde{M} = 7.9\,10^{14}\,M_o$
- *Planck final (30 months) mission*
  - *Consistency with theoretical models (Borgani et al., 04, Nagai et al, 07; Piffaretti & Valdarnini, 08); slight excess above* r_{500} *now detected beyond z=0.5*

Comparison with hydrodynamical simulations (Planelles et. al, 17)

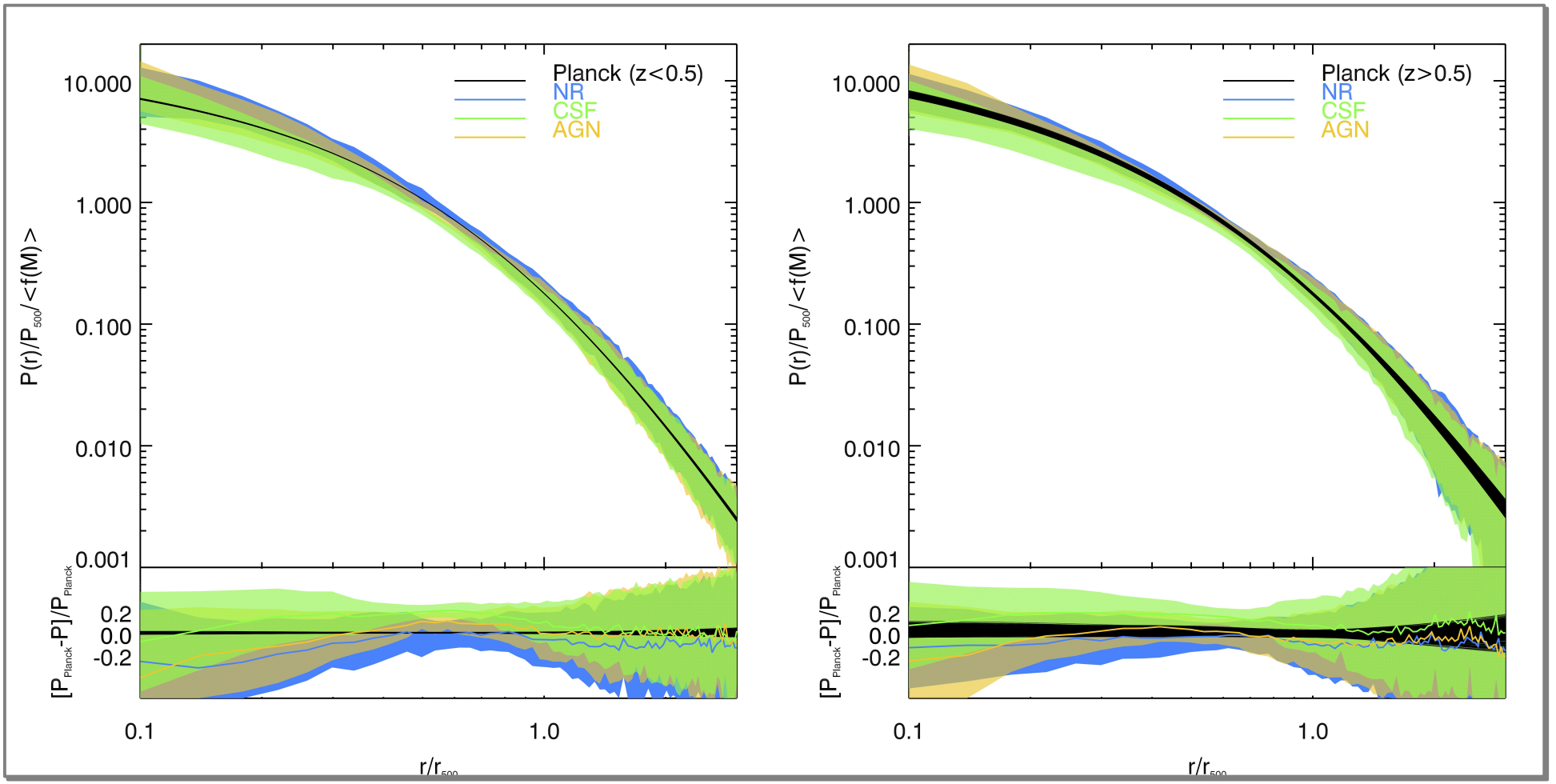

Spectroscopic X-ray vs. X-ray+SZ temperatures

z < 0.5
(z_{med}=0.15)

z > 0.5
(z_{med}=0.55)

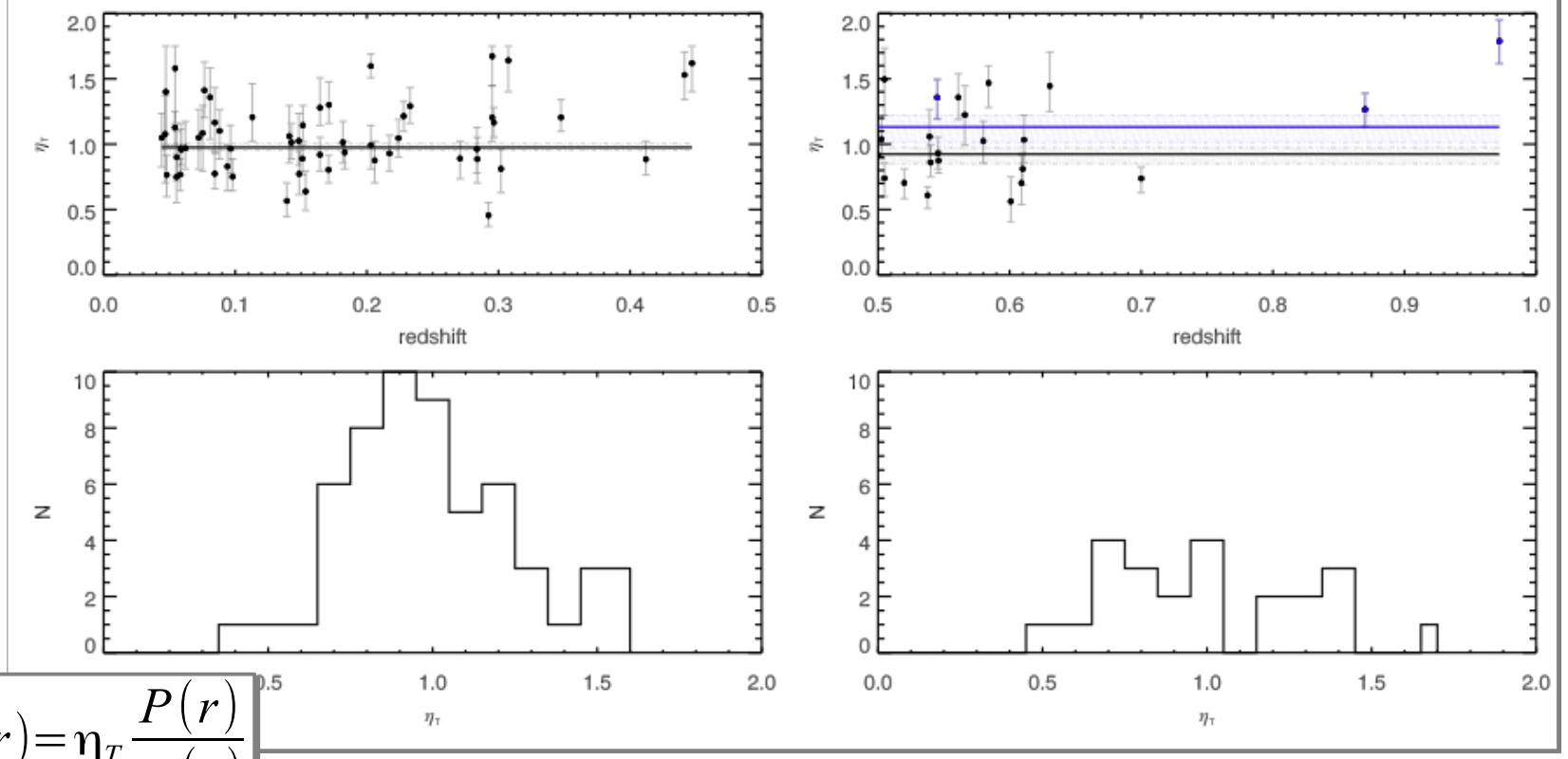

$$k\,T(r) = \eta_T \frac{P(r)}{n_e(r)}$$

Determination of the Hubble constant from nearby clusters (z<0.5) in the Planck catalogue

(Kozmanyan et al., 19)

$$k\,T(r) = \eta_T \frac{P(r)}{n_e(r)}$$

$$\eta_t = \left(\frac{\bar{D}_a}{D_a}\right)^{1/2} \times \left(\frac{n_p/n_e}{\bar{n}_p/\bar{n}_e}\right)^{1/2} \times \left(\frac{1+4\mathrm{n}_{He}/n_p}{1+4\,\bar{n}_{He}/\bar{n}_p}\right)^{1/2} \times \left(\frac{C_\rho}{\epsilon_{LOS}}\right)^{1/2}$$

$$H_o = 67 \pm 3\ km.s^{-1}.Mpc^{-1}$$

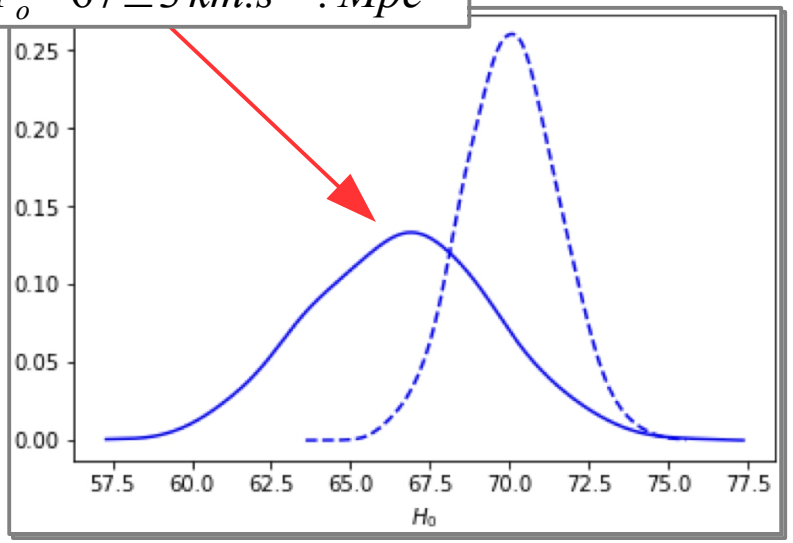

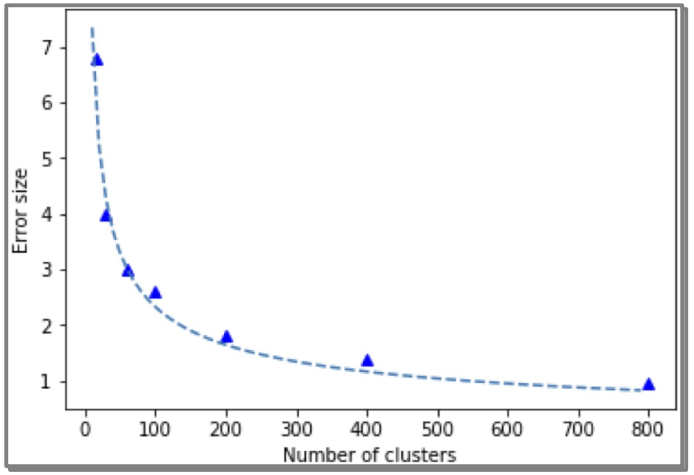

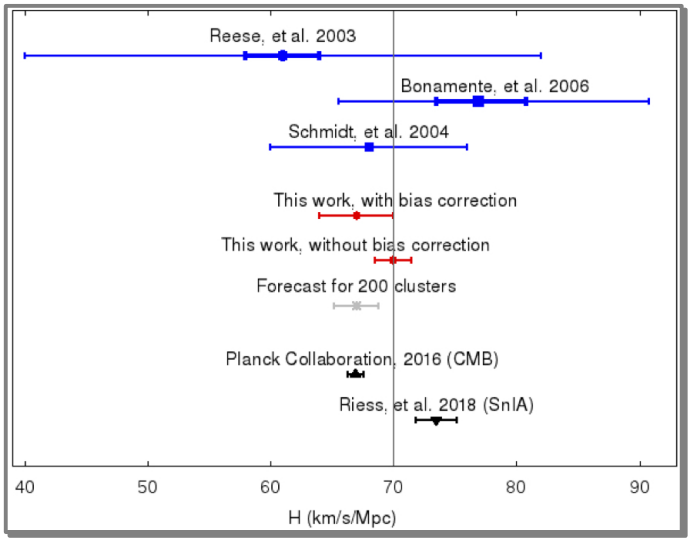

Cluster maps and substructure detection (Spectral-imaging)

Planck SI: component estimate

Uniform template (χ^2 estimate):

$$\chi^2 = \sum_{i,j,\nu} \frac{\left[I_\nu(i-k, j-l) - y_\nu(i-k, j-l) \right]^2}{\sigma_\nu^2(i-k, j-l)}$$

Spatially variable template (weighted χ^2 estimate):

$$w\chi^2 = \sum_{i,j,\nu} w(i,j) \frac{\left[I_\nu(i-k, j-l) - y_\nu(i-k, j-l) \right]^2}{\sigma_\nu^2(i-k, j-l)}$$

$$y = \mu(\theta)$$
$$\frac{\partial w\chi^2}{\partial \theta} = 0 \longrightarrow \mu(\hat{\theta}) = \frac{\sum_{i,j,\nu} w(i,j) / \sigma_\nu^2(i-k, j-l) I_\nu(i-k, j-l)}{\sum_{i,j,\nu} w(i,j) / \sigma_\nu^2(i-k, j-l)}$$

Planck SI: component imaging, wavelet transform

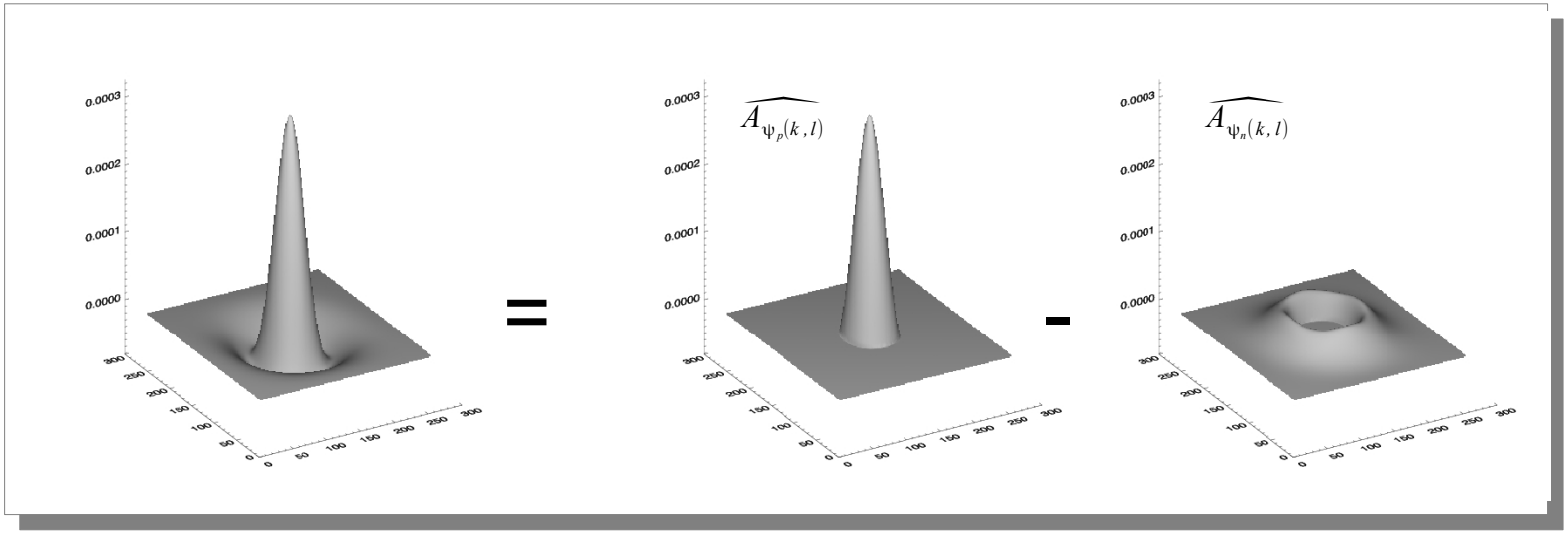

$$W(k,l,a) = \frac{1}{2} \times \left[\widehat{A_{\psi_p(k,l)}} - \widehat{A_{\psi_n(k,l)}} \right]$$

$$dW(k,l,a) = \frac{1}{2} \times \sqrt{\widehat{\sigma^2_{A_{\psi_n}(k,l)}} + \widehat{\sigma^2_{A_{\psi_p}(k,l)}}}$$

Variance stabilized transform: $W'(k,l,a) = \frac{W(k,l,a)}{dW(k,l,a)}$

Planck SI: component imaging, curvelet transform

B3-spline (à trous) wavelet analysis

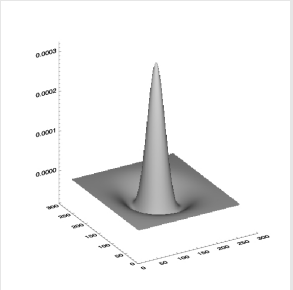

Ridgelet analysis

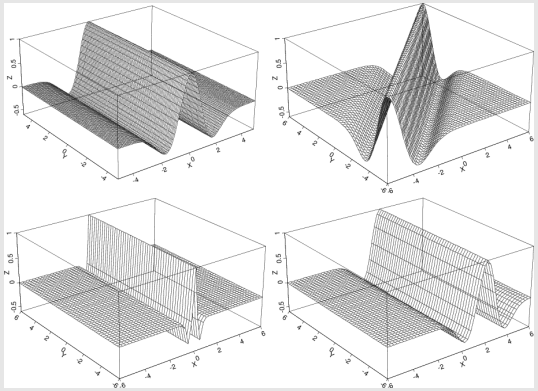

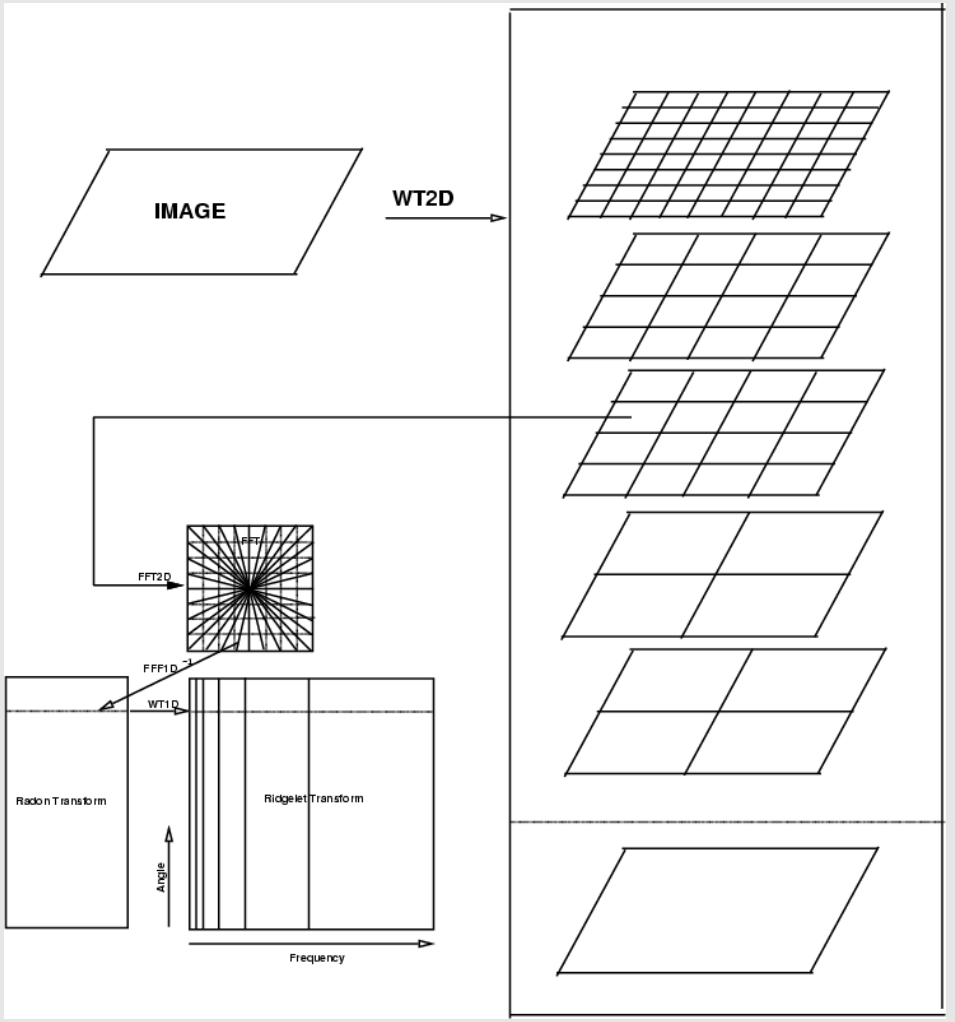

Starck, Donoho and Candès, 03

Sparse component restoration: denoising + van-Cittert deconvolution

Image denoising (wavelet and curvelet transform thresholding):

$$\widehat{\boldsymbol{A}}_{\boldsymbol{o}}(k,l)=f\left[argmin\left(w\chi^2[\boldsymbol{I}_{\boldsymbol{o}}]\right)\right]=\begin{bmatrix} R_W\bar{W}[1+A_{CMB}(k,l)] \\ R_C\bar{C}[A_{dust}(k,l)] \\ R_C\bar{C}[\log(1+A_{SZ})(k,l)] \end{bmatrix}$$

Image restoration -van-Cittert deconvolution within the *multiresolution support of* **A_n** *(Murtagh et al., 95)-:*

$$P*\boldsymbol{A}_{\boldsymbol{n}}=argmin\left(w\chi^2[P*\boldsymbol{I}_{\boldsymbol{n}}]\right)$$

$$\boldsymbol{R}_{\boldsymbol{n}}(x,y)=\boldsymbol{A}_{\boldsymbol{o}}(x,y)-[P*\boldsymbol{A}_{\boldsymbol{n}}](x,y)$$

$$\boldsymbol{A}_{\boldsymbol{n+1}}=\boldsymbol{A}_{\boldsymbol{n}}+\alpha\,\boldsymbol{R}_{\boldsymbol{n}}(x,y)$$

SZ map restoration w.r.t. noise variance

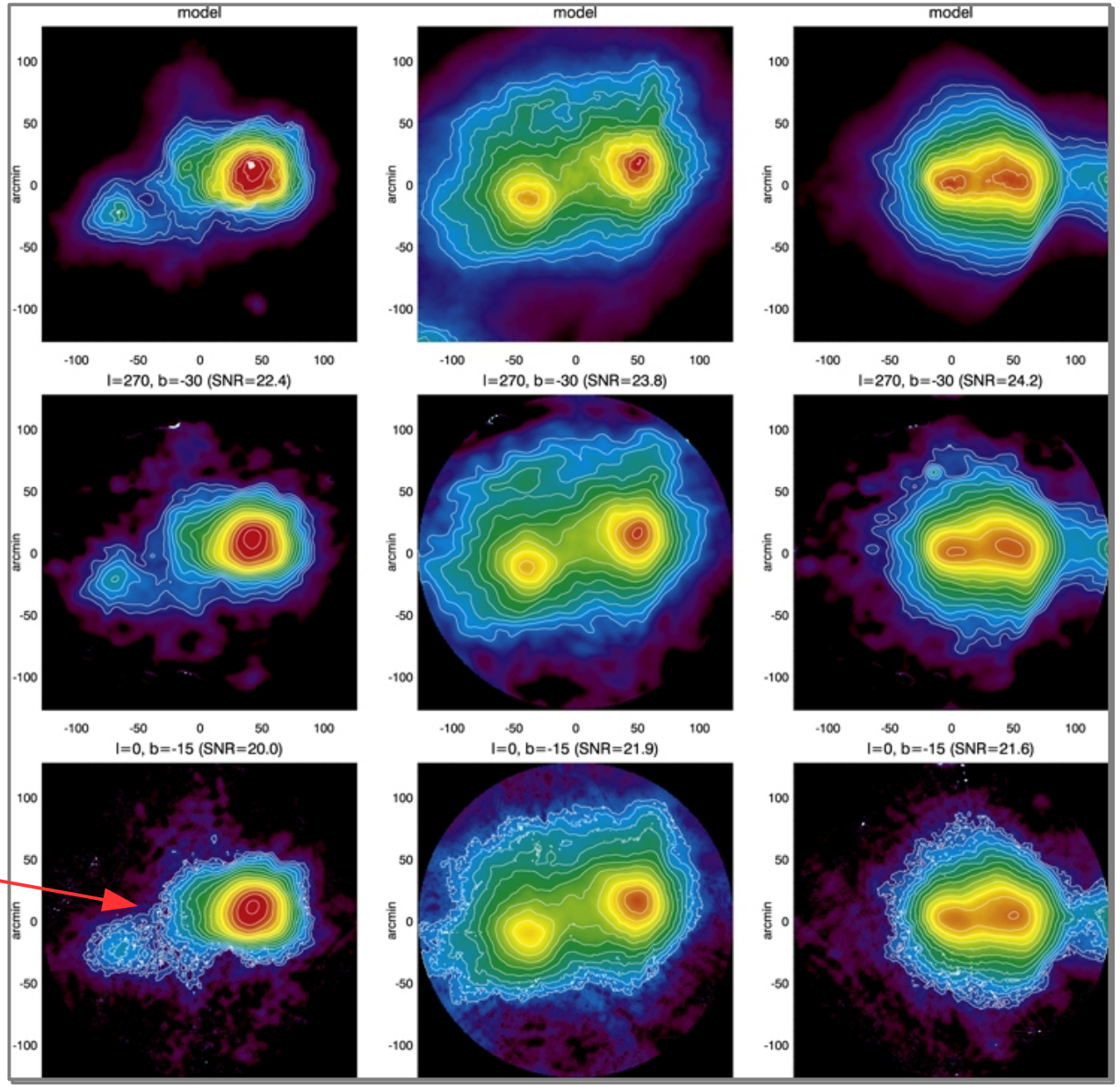

Expected SZ signal

High SNR sky region

Low SNR sky region

Thresholding + Deconvolution artifacts

Sparse component restoration: wavelet likelihood deconvolution

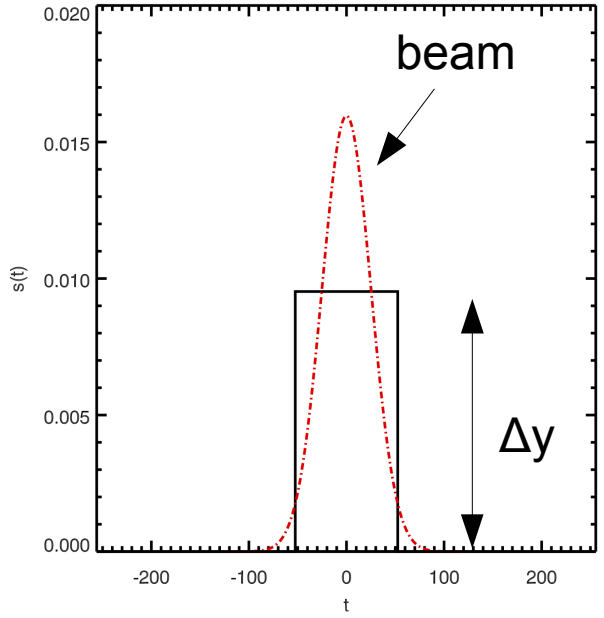

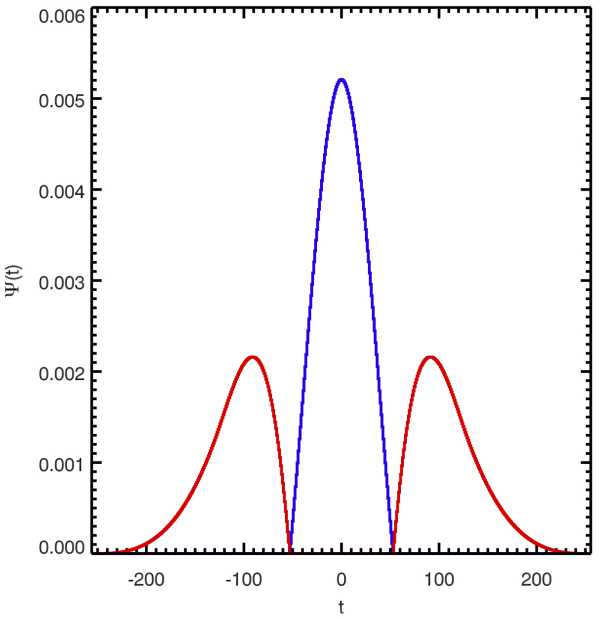

$$w\chi^2(\Delta y, t) = \sum_i w(i) \frac{\left[I(i-t) - H[y+\Delta y](i-t) - (1-H)[y-\Delta y](i-t) \right]^2}{\sigma_v^2(i-t)}$$

Sparse component restoration: wavelet likelihood deconvolution

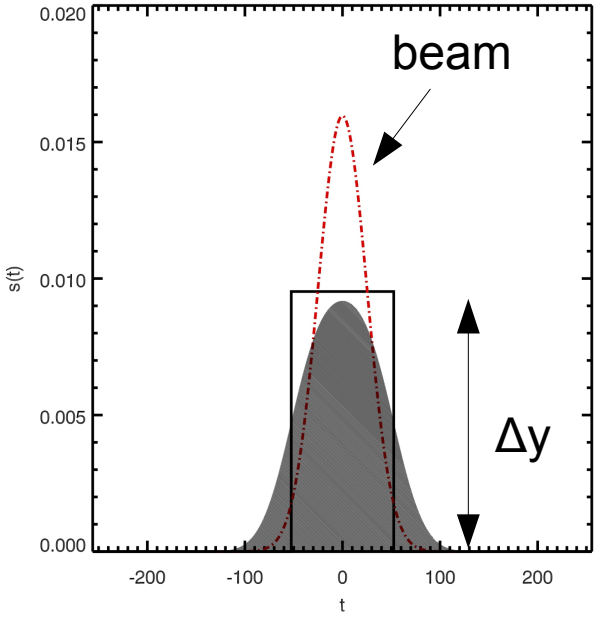

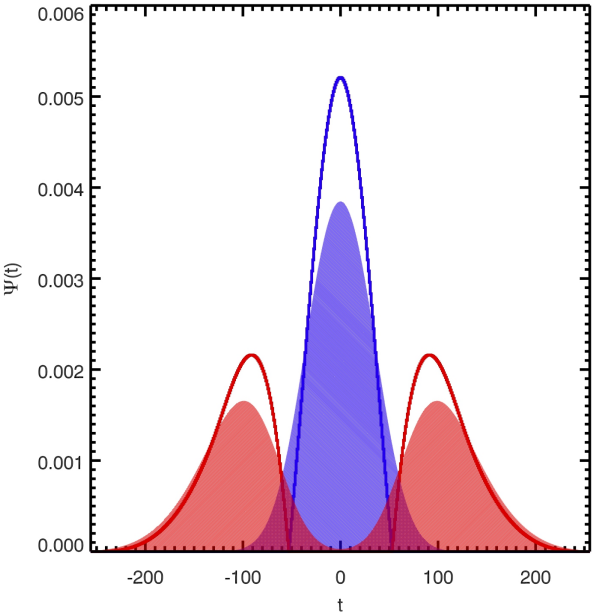

$$w\chi^2(t)=\sum_i w(i)\frac{\left[I(i-t)-b*H[y+\Delta y](i-t)-b*(1-H)[y-\Delta y](i-t)\right]^2}{\sigma_v^2(i-t)}$$

A3395-A3391 bridge

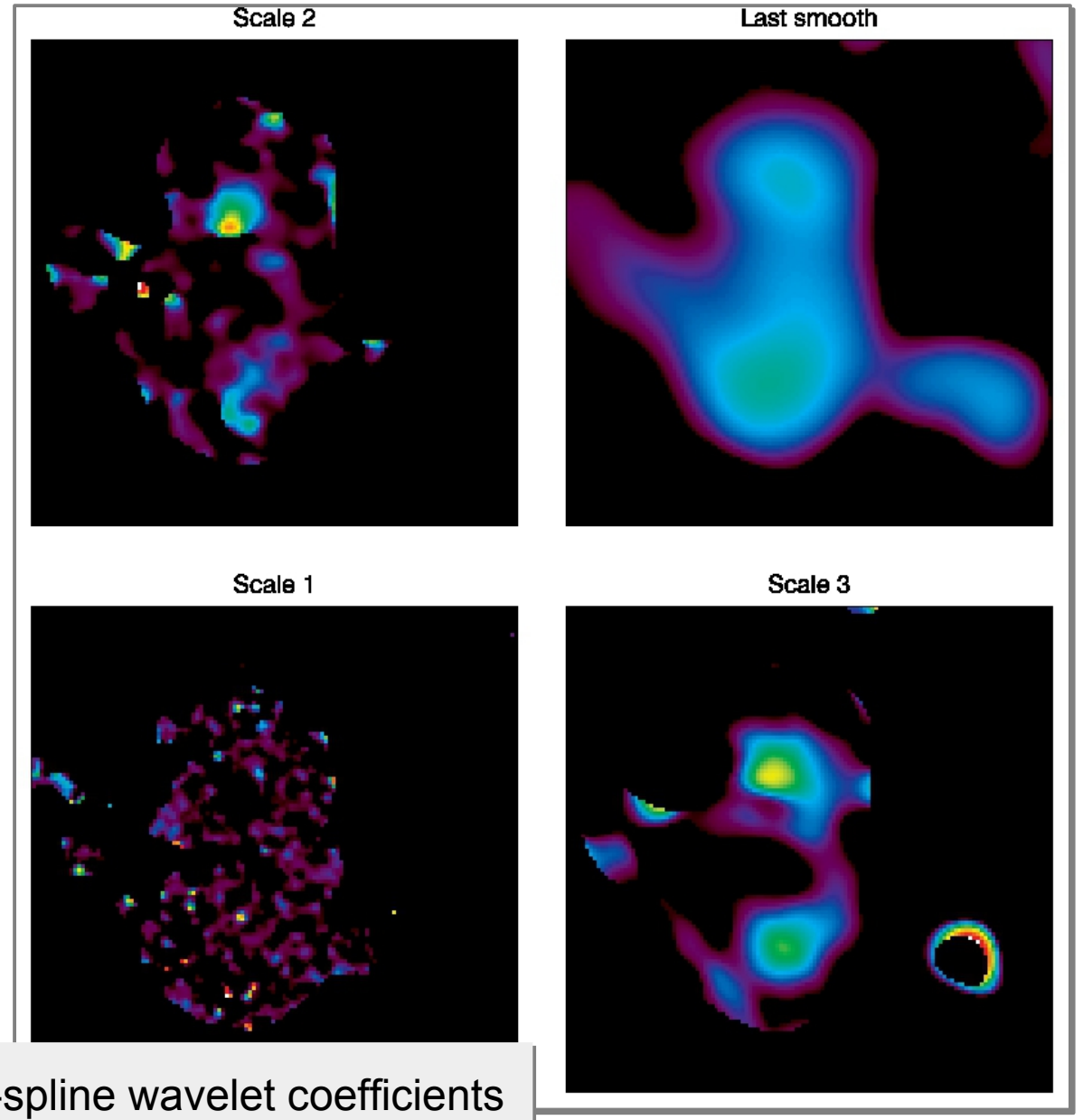

B3-spline wavelet coefficients

A3395-A3391 bridge

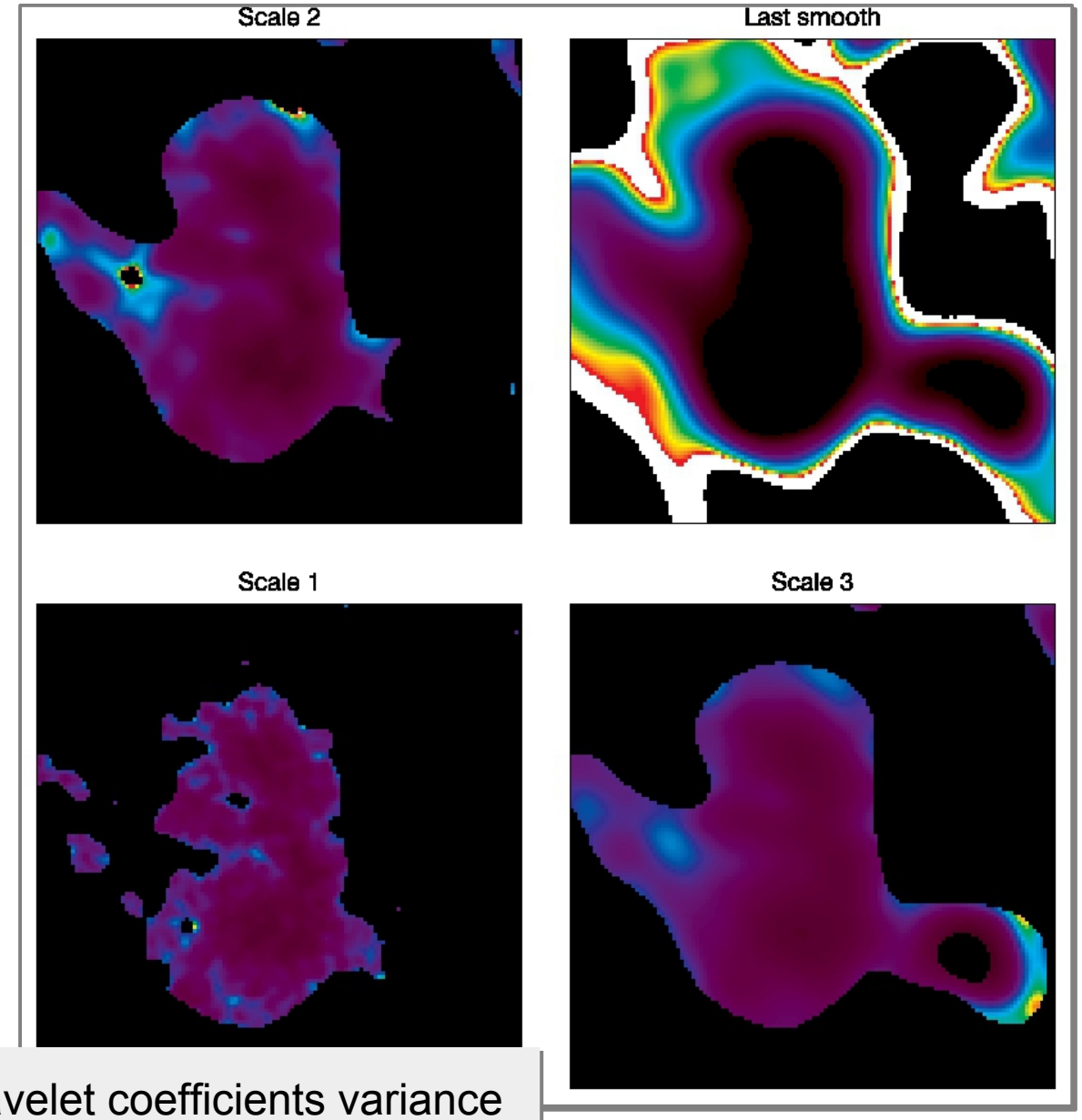

wavelet coefficients variance

A3395-A3391 bridge

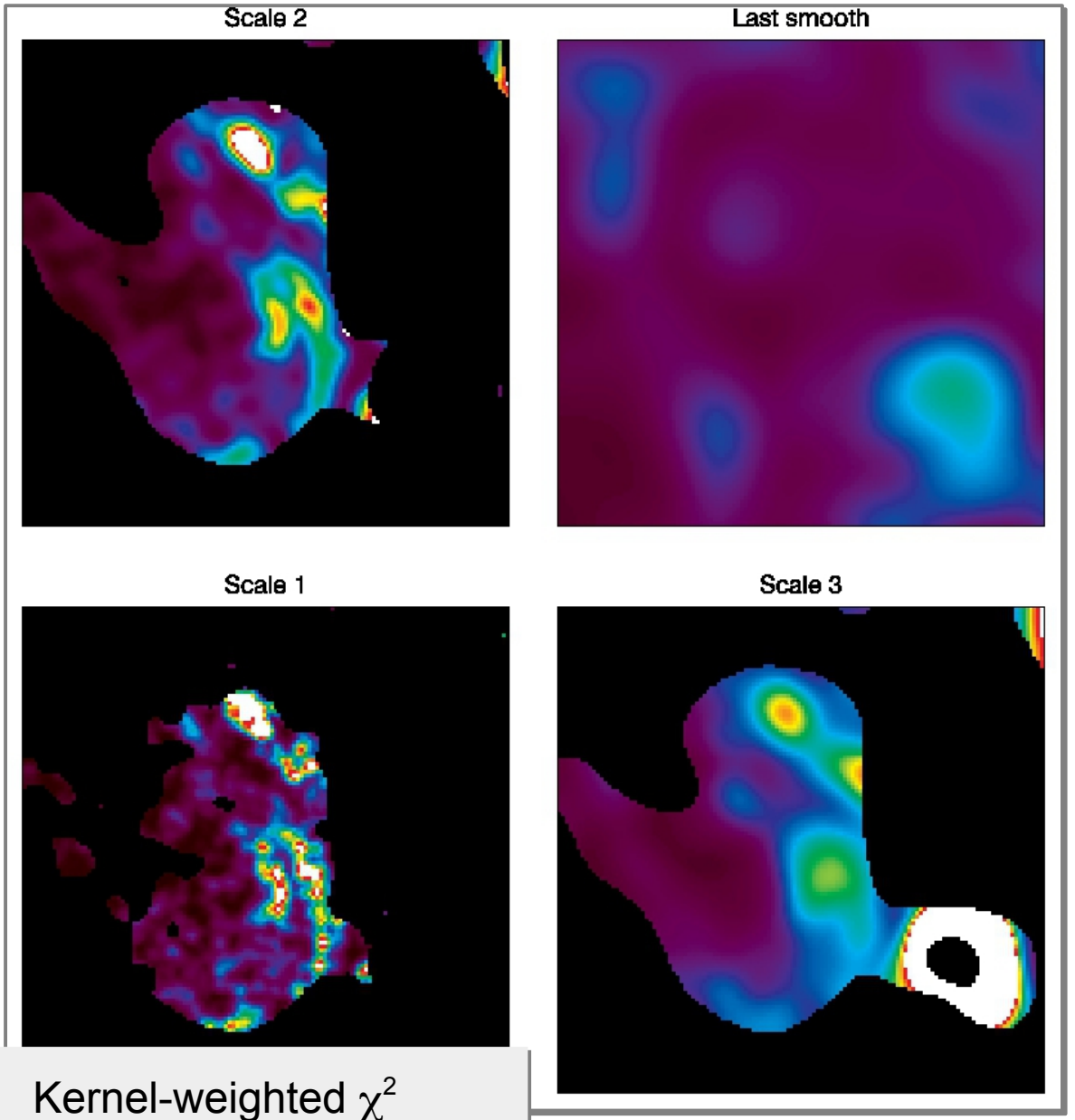

Kernel-weighted χ^2

A3395-A3391 bridge

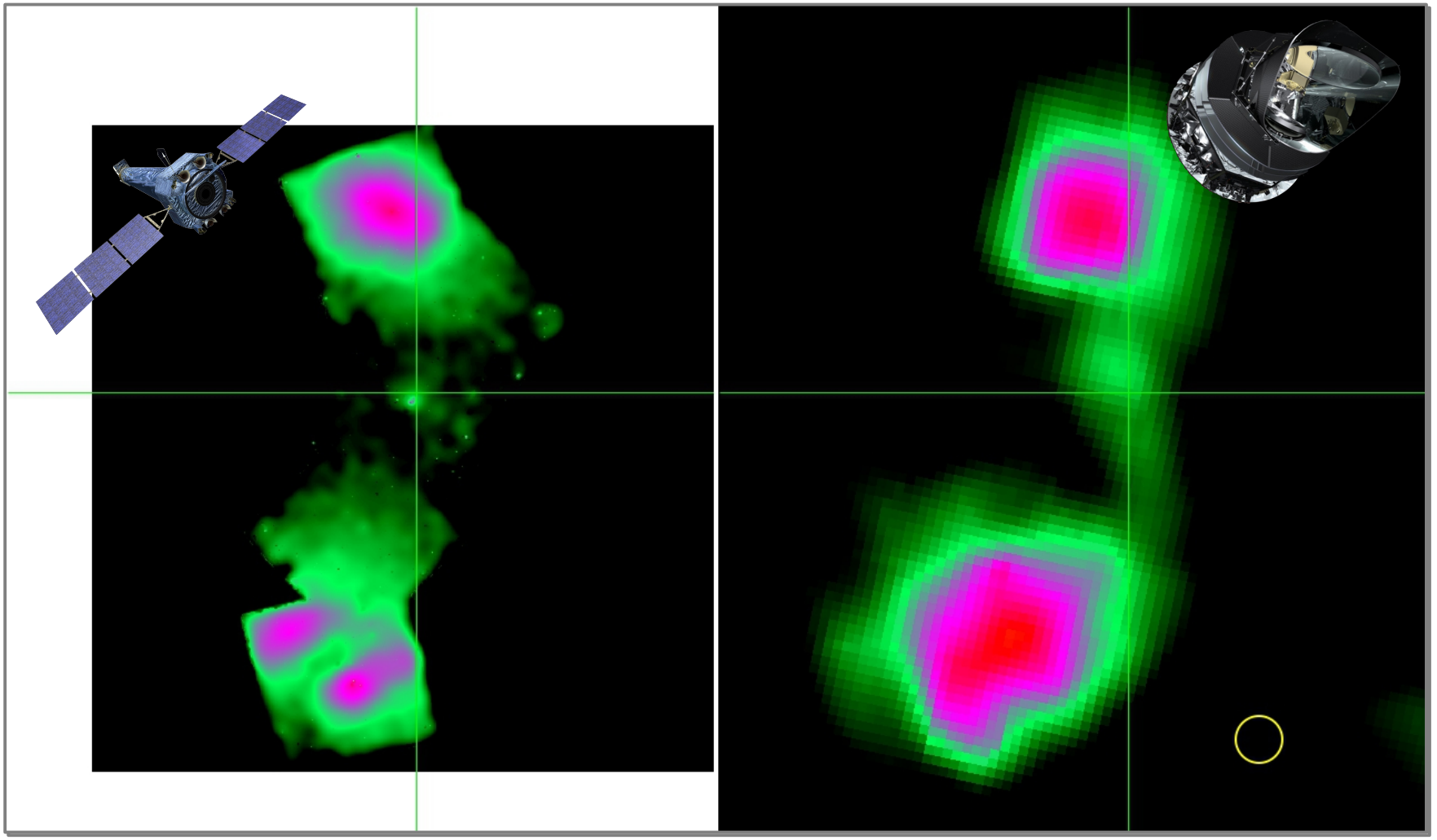

A3667 – A754 (shock front clusters)

- Shocks are surprisingly hard to evidence with *Planck;*
- Peripheral structures and filaments are detectable;

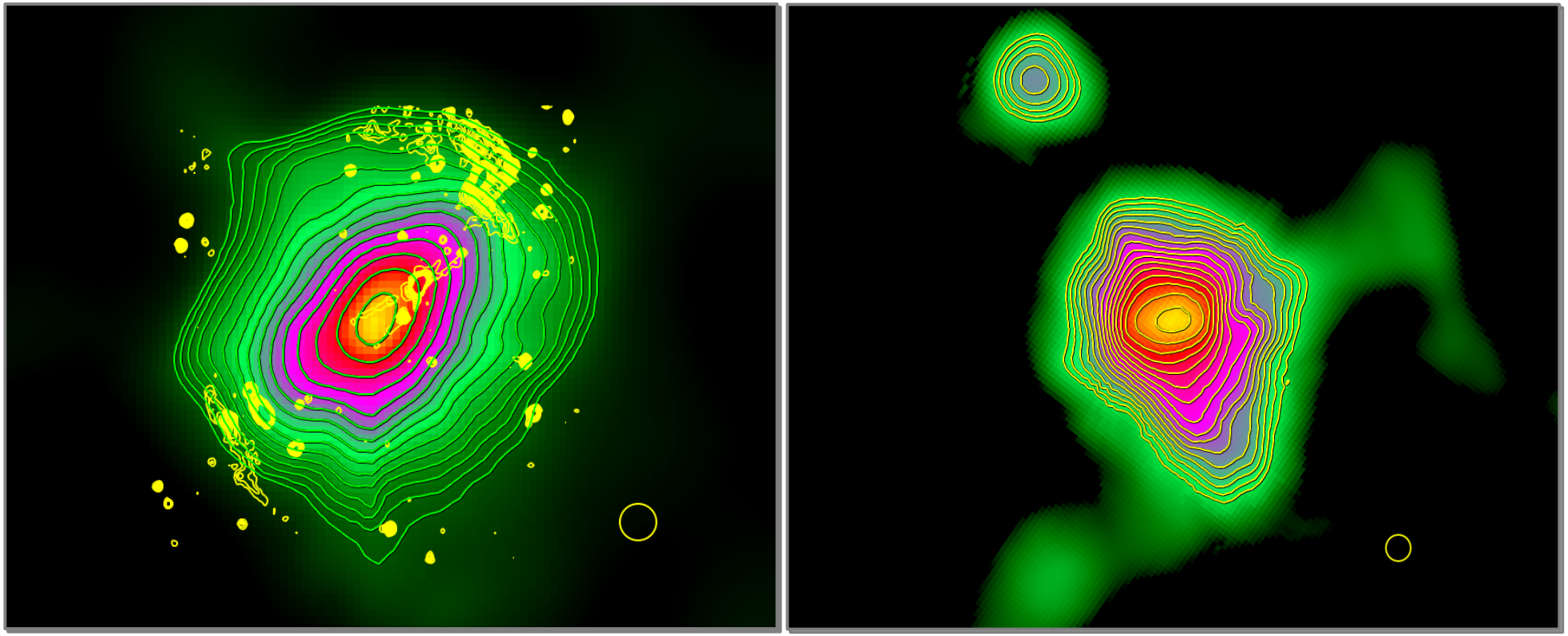

X-ray Cluster Outskirts Project

(P.I. D. Eckert; Baldi et al., in prep.)

- *XMM follow-up of the 12 highest SNR clusters of the MMF3 catalogue;*
- *Peripheral structures are detectable for* $r_{500} < r < r_{200}$.

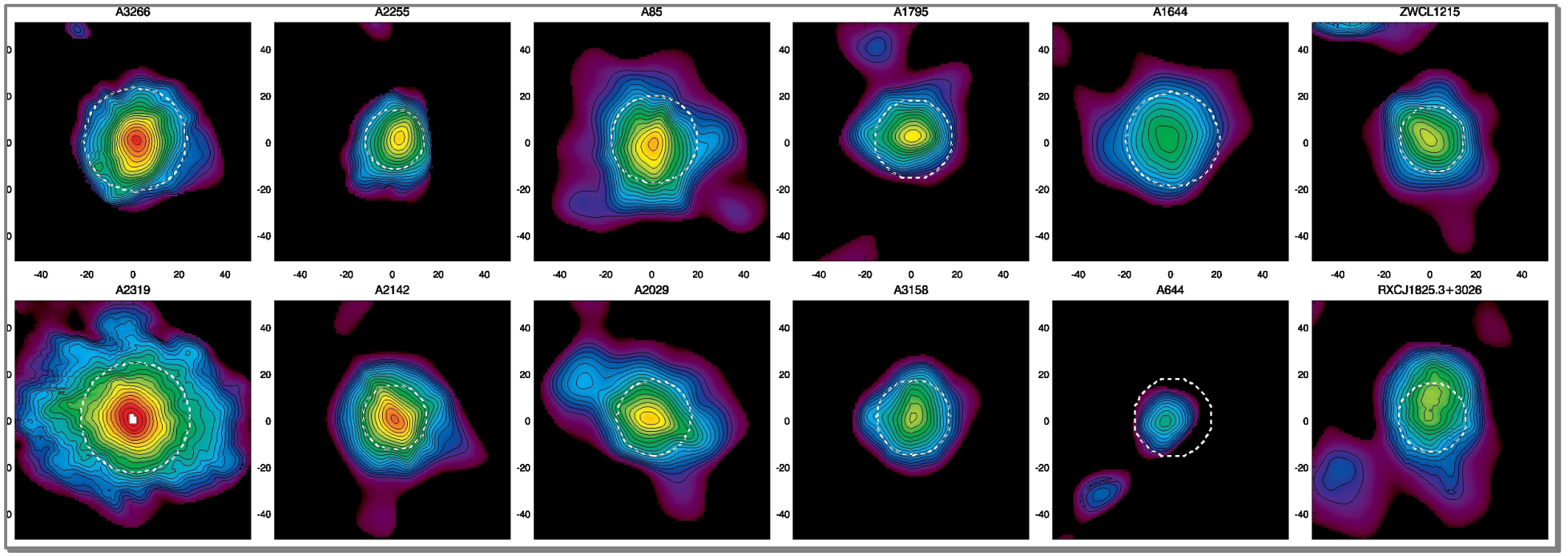

All sky Compton parameter (10 arcmin smoothing)

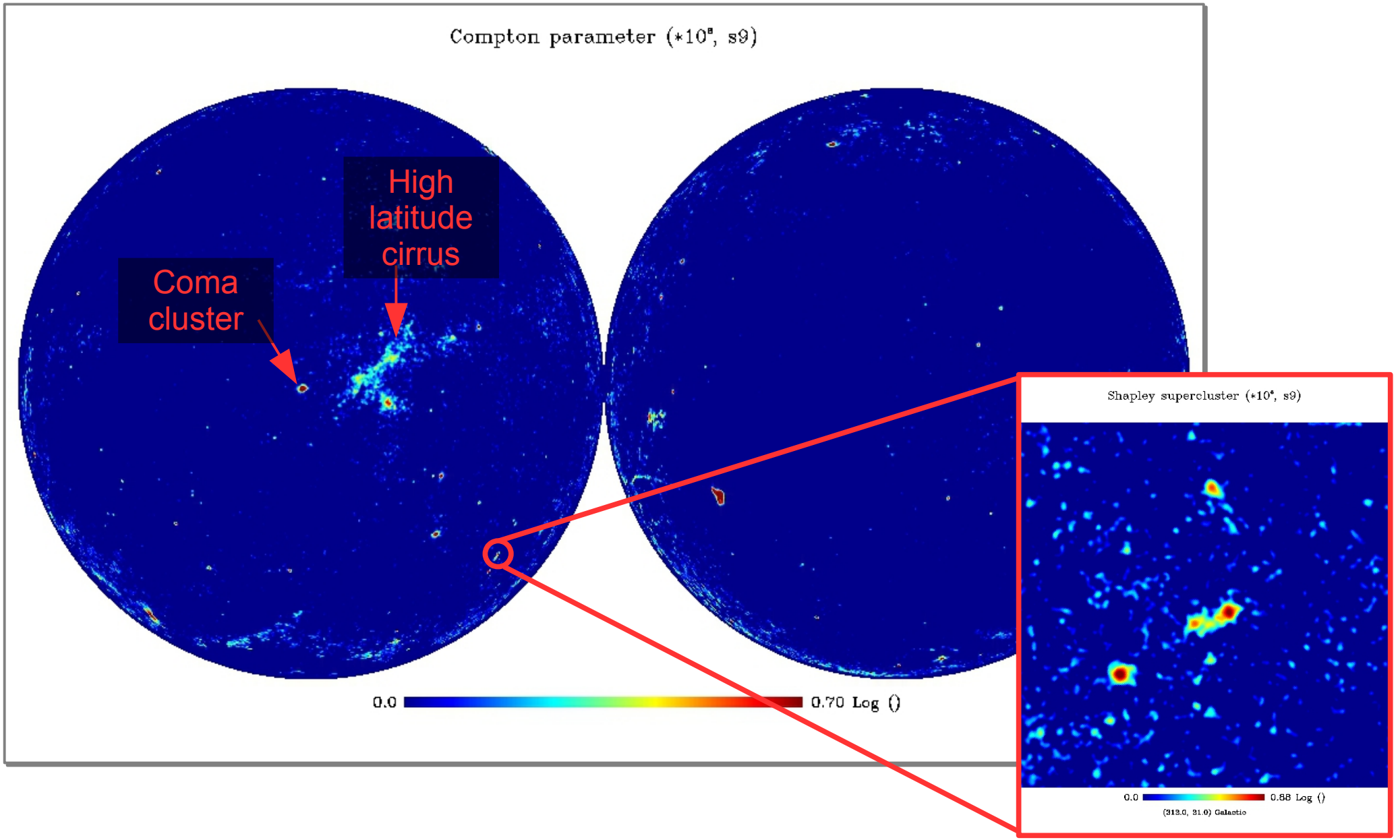

Toward new cluster detections (wavelet denoised matched filters)

Stacking Planck data toward anciliary cluster catalogues (future detections?)

Meta-Calatogue of X-ray clusters

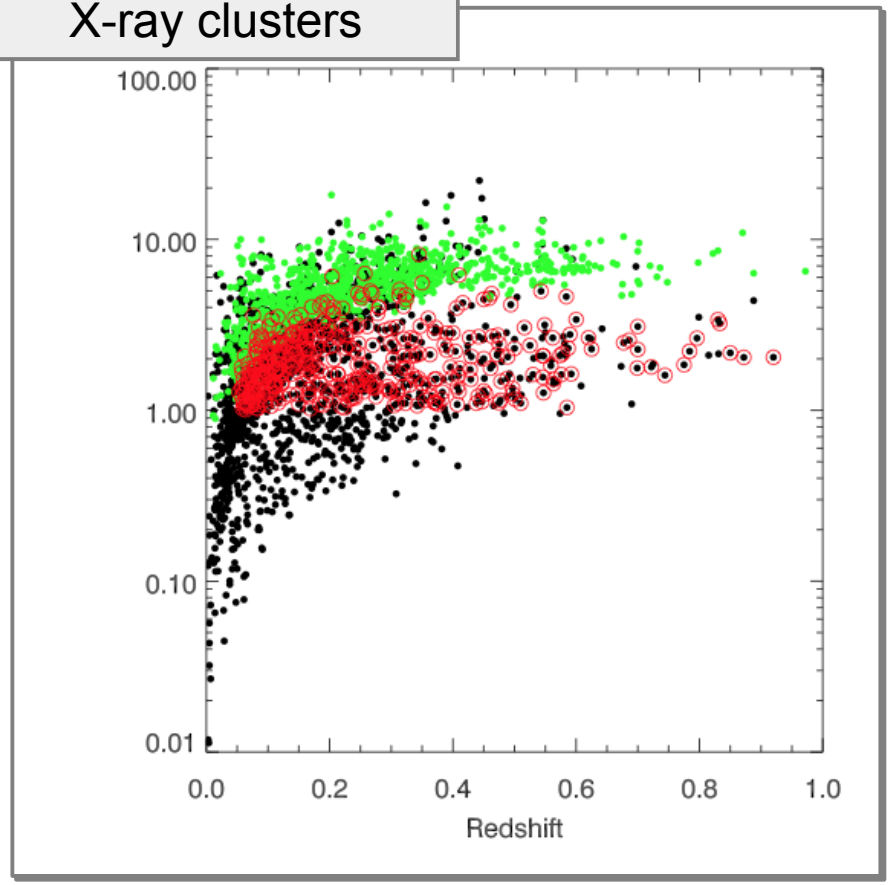

South Pole telescope catalogue

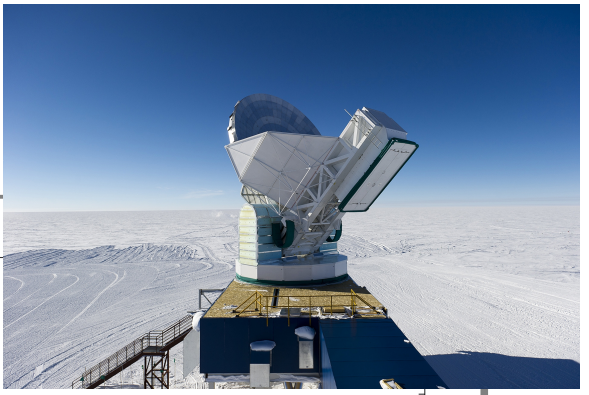

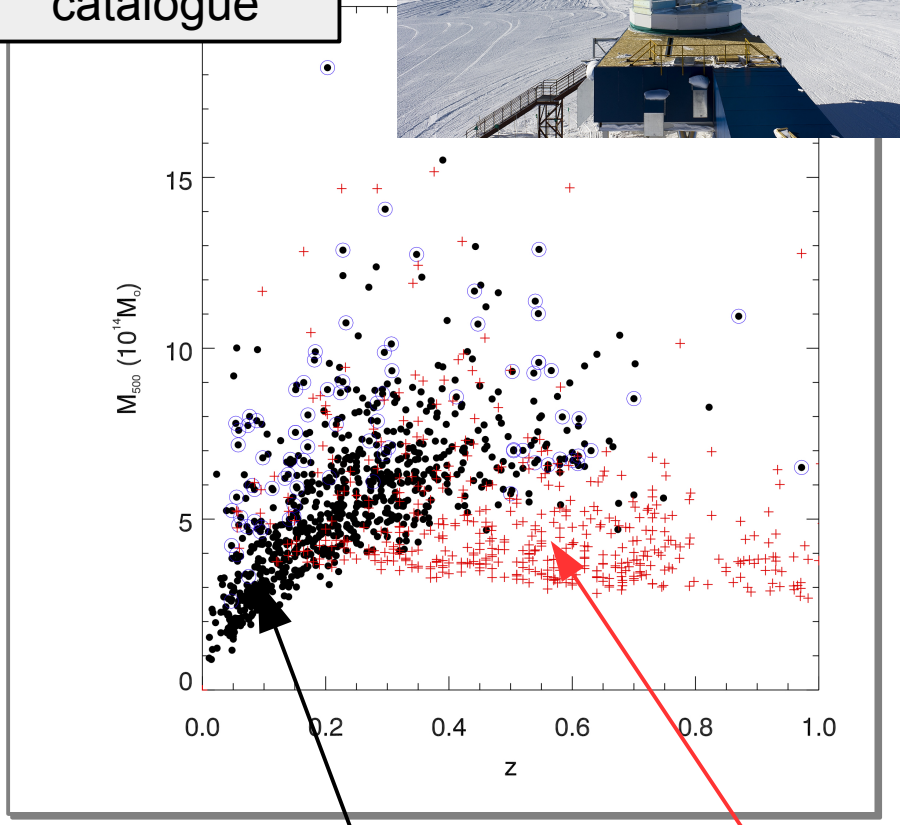

Planck

SPT

Stacking Planck data toward anciliary cluster catalogues (future detections?)

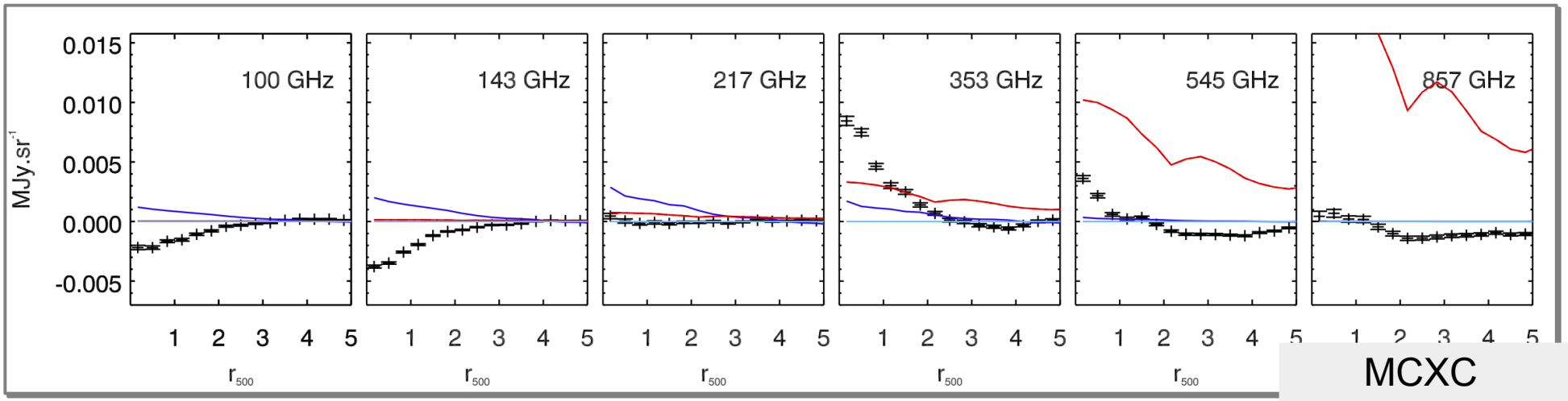

MCXC

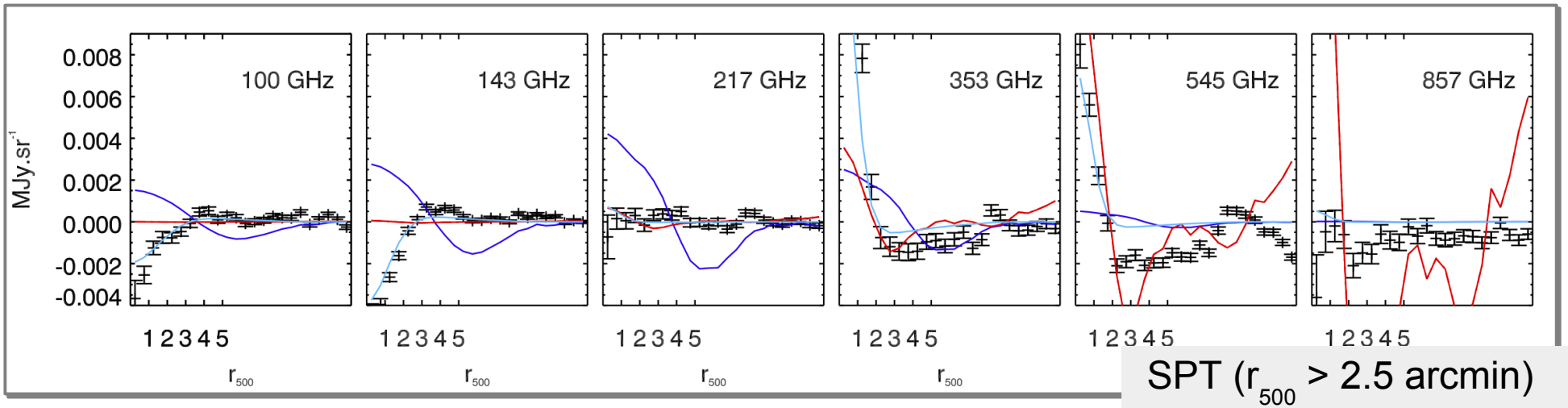

SPT (r_{500} > 2.5 arcmin)

Conclusions - perspectives

- Pressure profile of *Planck* detected clusters:
  - Sparse representations of contaminants (three component thermal dust + CMB + thermal SZ template) allow us to recover pressure profiles of nearby and distant clusters in the *Planck catalogue*

    --> little or no evolution of the pressure profile shape with redshift;

    --> joint X-ray+SZ analysis allow us to constraint Ho with 4% accuracy, with prospects for improvements with more clusters (XMM, Chandra, e-Rosita follow-ups?).
- Maps of the thermal SZ signal (from cluster patches to full sky):
  - *Planck 2018 data motivated the development of component separation algorithms that can combine heterogeneous beams, energy bandpass and noise models; such algorithms allow us to detect structures in the peripheries of nearby clusters; next step should be the combination Planck frequency maps with higher resolution data sets;*
- Toward new cluster detections:
  - *Selection function of the Planck cluster catalogue is not strictly mass dependent;*
  - *Wavelet denoised matched filters might reveal clusters hidden within CMB or thermal dust anisotropies.*

All sky thermal dust (10 arcmin smoothing)

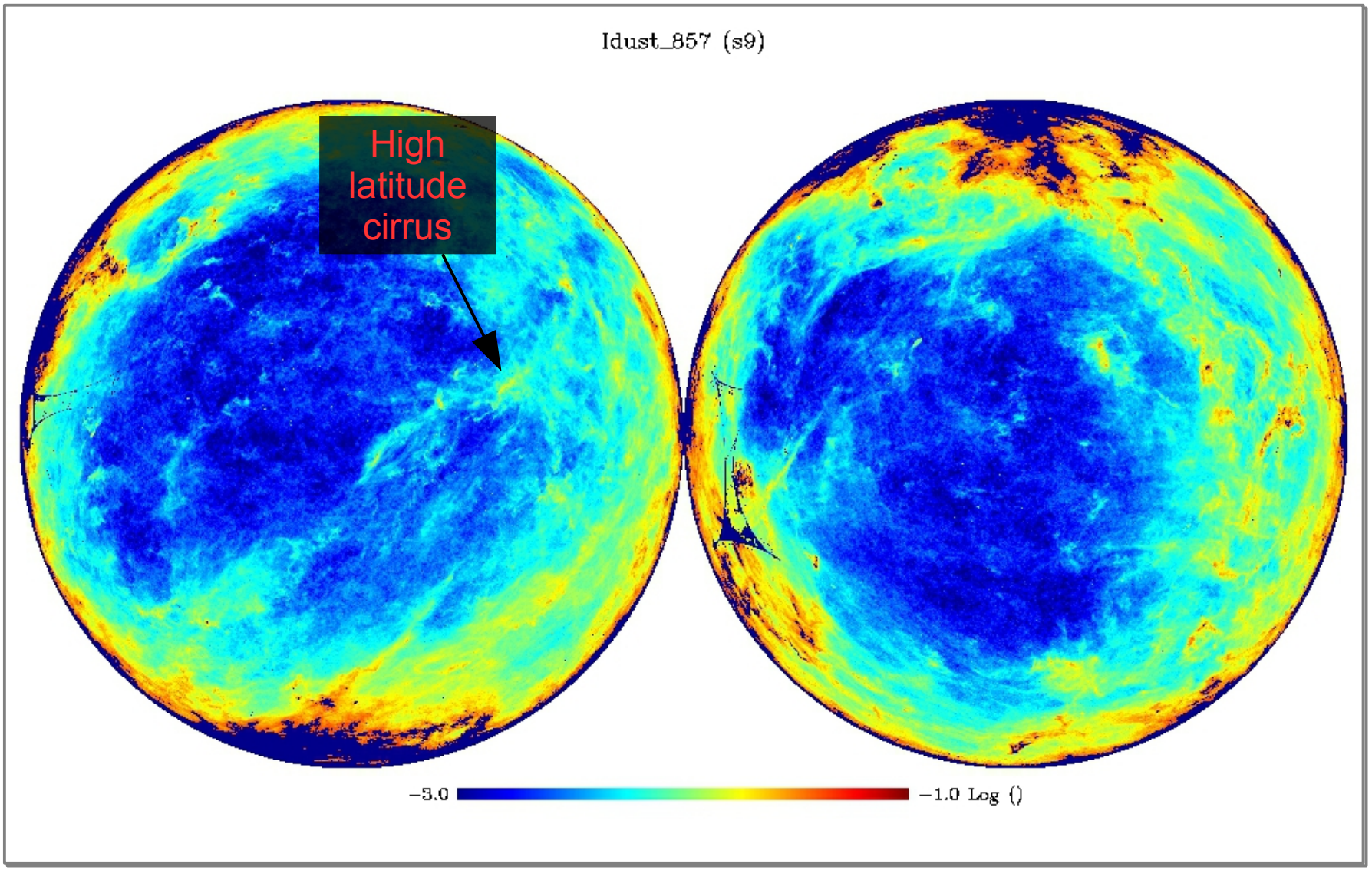

All sky CMB (10 arcmin smoothing)